Multilayer Graphene Rubber Nanocomposites

Inaugural-Dissertation

to obtain the academic degree

Doctor rerum naturalium (Dr. rer. nat.)

submitted to the Department of Biology, Chemistry and Pharmacy

of Freie Universität Berlin

by

DANIELE FRASCA

from Colleferro (IT)

2016

This PhD-Thesis was conducted from January 2013 to April 2016 at the Bundesanstalt für Materialforschung und -prüfung (BAM) (Berlin) under the supervision of Priv.- Doz. Dr. rer. nat. habil. Bernhard Schartel.

1st Reviewer: Priv.-Doz. Dr. rer. nat. habil. Bernhard Schartel, Bundesanstalt für Materialforschung und -prüfung (BAM) (Berlin).

2nd Reviewer: Prof. Dr. rer. nat. Rainer Haag, Freie Universität Berlin.

Date of Defense: 12.09.2016

to Silvia

"Su coraggio, chi ha una spada la affili"

Stefano Benni

Acknowledgements

First of all I would like to thanks Priv.-Doz. Dr. rer. nat. habil. Bernhard Schartel for giving me this great opportunity to conduct my PhD research in his group. He always supports me and gives me scientific suggestions to fulfill my PhD work.

I also thank Prof. Dr. rer. nat. Rainer Haag for reviewing this work.

Naturally I have to thank several others people of the division 7.5 of the BAM: the "Gummi Team" (Dietmar, Carsten, Bernd and Jeannette), Dr. rer. nat. Böhning, Dr. rer. nat. Wachtendorf, Thommy, Patrick and the guys of the workshop.

I cannot forget my "Travel Fellowship" led by Michael and Sebastian, and including: Analice, Benjamin, Sebastian, Nora, Karoline, Marie-Claire (Loulou), Marie-Bernadette, Antje, Kirsten, Huajie, Patrick, Andreas, Alexander, Tim, Lars, Angelo, Salvatore, Elizabeth, Yuttapong and Weronika.

A special thanks to my wonderful officemates Aleksandra, Bettina and Melissa.

I want to thank my formal collegues of the "Marangoni", Massimo, Sabrina, Antonio, Antonio, Stefano, Paolo, Gaetano, Angelo and Fabio.

My parents and my family were geographically far away but anyway close to me like my brother, his partner Franziska and their kids (Fabio and Caterina), and my girlfriend Anna.

Now it is time to thank all my Italian friends, starting with the "Shit Friends" (Jackone, il Maestro, la Bestia di Seitan, Gommo, Riccardone, Lord e Amedeo), the guys of the "FantaPerMnganese" and "FantaQuessi", my old friends of Colleferro (Emanuele, Yuri, Ciccio, Francesco, Emanuele, Riccardo, Michela, Michela, Silvia and Eleonora) and my dear University colleagues (Augusto, Roberto, Matteo, Daniela, Paola, Carmela, Marialuisa, Barbara e Federica).

In the end I would like the thanks my “Culopesantici” friends in Berlin and moreover Andrea, Marco, Mattia, Lorenzo, Veronica, Carolina, Oana and Martina fantastic people that enjoyed with me the life in *Beerlin*.

Table of Contents

Abbreviations

BET	Brunauer Emmet Teller
CB	Carbon Black
CIIR	Chlorine Isoprene Isobutyl Rubber
CNT	Carbon Nanotubes
CR	Polychloroprene
CVD	Chemical Vapor Deposition
EHC	Effective Heat of Combustion
EG	Expanded Graphite
EPDM	Ethylene Propylene Rubber
G’	Storage Modulus
GO	Graphene Oxide
HRR	Heat Release Rate
IIR	Isoprene Isobutyl Rubber
LS	Layered Silicate
MAHRE	Maximum Average of Heat Emission
MBTS	Mercaptobenzthiazole Disulfide
MH	Maximum of the Torque
ML	Minimum of the Torque
MLG	Multilayer Graphene
MMT	Montmorillonite
MWCNT	Multiwall Carbon Nanotubes
NBR	Nitrile Butadiene Rubber
NR	Natural Rubber

phr	Part per Hundred Rubber
PHRR	Peak of Release Rate
SBR	Styrene Butadiene Rubber
SEM	Scanning Electron Microscopy
SWCNT	Singlewall Carbon Nanotubes
t_{100}	Time corresponding to 100 % of the Curing
t_{90}	Time corresponding to 90 % of the Curing
THE	Total Heat Evolved
TEM	Thermal Electron Microscopy
T_g	Glass Transition Temperature
t_{ig}	Time of Ignition
t_{s1}	Scortch Time
ΔS	Difference between Maximum and Minimum of the Torque
η'	Dynamic Viscosity

1.1 General Aspects of Rubbers

Rubbers, also called elastomers, are one of the most important commercial polymers. Raw elastomers are amorphous polymers with glass transition temperatures much lower than the ambient temperature. Rubbers have unique properties such as high elasticity, high deformability and low hardness. As thermoplastic polymers, raw elastomers become pliable and melt under heat, and solidify upon cooling; moreover, they can accept high loading of fillers. Elastomers can have a saturated structure (i.e. without double bonds carbon-carbon) such as polychloroprene (CR) and ethylene propylene rubber (EPDM) or an unsaturated structure (i.e. with double bonds carbon-carbon) such as natural rubber (NR), chlorine isoprene isobutyl rubber (CIIR), nitrile butadiene rubber (NBR) and styrene butadiene rubber (SBR) [1-3].

The polymeric chains in rubbers are long, flexible and linear (i.e. without lateral groups) with a strongly coiled and random structure (Fig.1a). Under stress, the elastomeric chains uncoil in a stretched aligned structure, hence the rubber structure becomes less disordered and the system looses entropy. Upon release of the stress, the molecules recover their initial coiled and random structure, which results in an increase in entropy. In conclusion, the entropy leads to the elasticity of the rubbers [4]. Since the polymeric chains are free and they move independently of each other, raw rubbers are elastic only at small deformations.

Elasticity and other properties of raw elastomer are improved by means of a cross-link reaction, called vulcanization, between the polymeric chains. Fig.1b shows a vulcanized elastomeric coil with a reticulate structure similar to a thermoset polymer. After vulcanization the elastomeric chains cannot move independently from each other anymore. Thus, vulcanized rubbers are elastic also at big deformations and have better mechanical properties.

Furthermore, vulcanized elastomers present higher resistance against heat, aging and chemicals.

Raw rubbers are always vulcanized in their application in the real life, such as tires, tubes, shoes, gloves and seals [1-3].

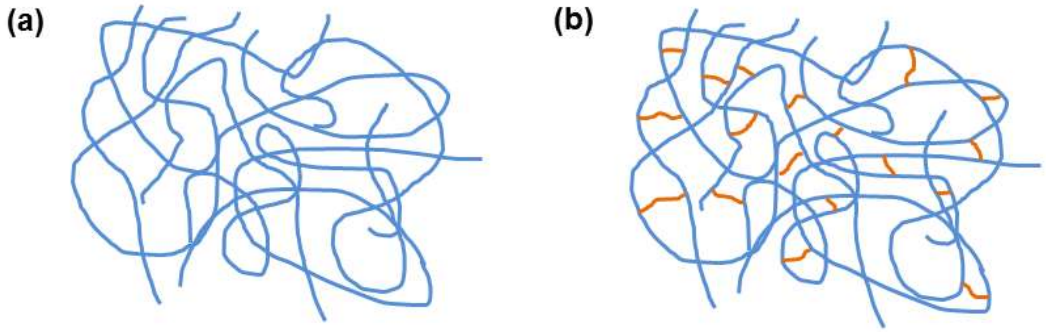

Fig. 1 – (a) raw elastomeric coil; (b) vulcanized elastomeric coil, the orange lines represent the sulfide bridge.

The vulcanization of unsaturated elastomers runs at high temperature, under high pressure and in presence of curing agents: the most popular cross-linker is the rhombic sulfur; zinc oxide and stearic acid are the activators while benzothiazoles, benzothiazolesulfenamides and thiurams are the typical accelerants [1-3].

The vulcanization of elastomers is schematized in Fig. 2; this process includes several reactions which can be divided in three main groups [5,6]:

i. The first step (called accelerators chemistry or induction time) includes the formation of an active accelerator complex through a reaction between the accelerators and the activators, which subsequently reacts with sulfur to form an active sulfarating agent.

ii. In the second step (called crosslinking chemistry) the active sulfarating agent reacts with an allylic carbon of the elastomeric chain to form a rubber

vulcanization precursor. This then reacts with an unsaturated site of another elastomeric chain, resulting in polysulfide crosslink.

iii. During the third and final step (post-crosslinking chemistry) the polysulfide crosslinks undergo a desulfuration to the more stable mono and disulfidic crosslinks.

Alternatively, the vulcanization can be realized using peroxides as crosslink agents. Peroxides react with elastomers by removing hydrogen atoms from the polymeric chains, creating highly active sites on the chain, which attach to a similar site on another chain, resulting in a carbon to carbon cross-link. Saturated elastomers are usually vulcanized with peroxides [1-3].

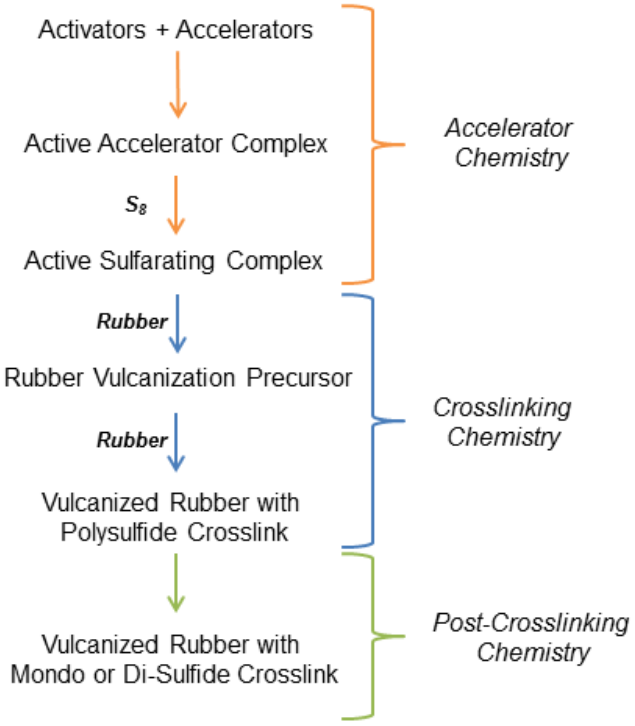

Fig. 2 – General mechanism of the vulcanization of unsaturated rubbers using rhombic sulfur as cross linker.

1.2 Rubber Composites

In all their applications, rubbers are filled and reinforced with high concentrations (above 40 phr) of small and hard particles in order to improve the mechanical properties such as hardness, elastic modulus and abrasion resistance, and functional properties such as gas barrier, electrical and thermal conductivity [7,8]. Several factors play a role in the reinforcing of elastomers: the geometrical characteristics of the filler (such as size and aspect ratio), the intrinsic properties of the filler (such as elastic modulus and electrical conductivity), the interactions between rubber and filler, the orientation, the dispersion and the concentration of the filler in the elastomeric matrix [9].

Among the fillers, carbon black (CB) was the first used as reinforcing filler in 1904, and since then CB has been widely used in rubber industry. CB consists of carbon in the form of spherical particles with colloidal size; moreover the surface of the particle presents carboxylic and hydroxyl groups. The fine particles of CB always coalesce into aggregates, which are in an irreversible and anisometric form; these aggregates tend to attract to each other by van der Waal bonds, forming loosely-bounded agglomerates. Fig.3 shows an illustration of a CB agglomerate. The agglomerates are broken during the mixing process of the rubber and CB results usually well dispersed in rubber composites [10].

Fig. 3 – Schematic illustration of a CB agglomerate.

CB is produced by partial combustion or thermal cracking of heavy petroleum products (furnace black) or natural gas (thermal black). A production reactor consists of two zones: high temperature zone, to break the hydrocarbons produced by fuel, and quenching zone, to stop the reaction by adding water. The reaction time is controlled by quenching, which determines the morphology of the products. Small-size CB is produced by short reaction time at high temperature [1,3].

Since the 50s, precipitated silica has been used as a filler for rubber. It is an amorphous form of silicon dioxide produced by reacting sodium silicate solution with either sulfuric acid. Silica consists of silicon and oxygen arranged in a tetrahedral structure of three-dimensional lattice. Silica particles present a spherical shape and on their surface there are several silanol groups which form hydrogen bonds to each other, hence very strong filler-filler interactions. Thus, the particles of silica always form aggregates and successively agglomerates[1,3].

Because of its polar nature and the strong filler-filler interactions, the dispersion of silica in rubbers is very poor. It is usually improved by a surface modification, through the introduction of appropriate functional groups by chemical reactions. The tetrasulfide-silane is widely used for the modification of silica in rubber compounds because they are compatible with the chemical nature of both the filler and the elastomeric matrix. The alkoxy groups of the silane react with the silanol groups of the silica particles, improving the compatibility between rubber and silica, and hence the dispersion of the filler, whereas the polysulfide groups react with the elastomeric chain during the vulcanization process [1,3,11]. The reaction between silica, tetrasulfide-silane and rubber is illustrated in fig. 4.

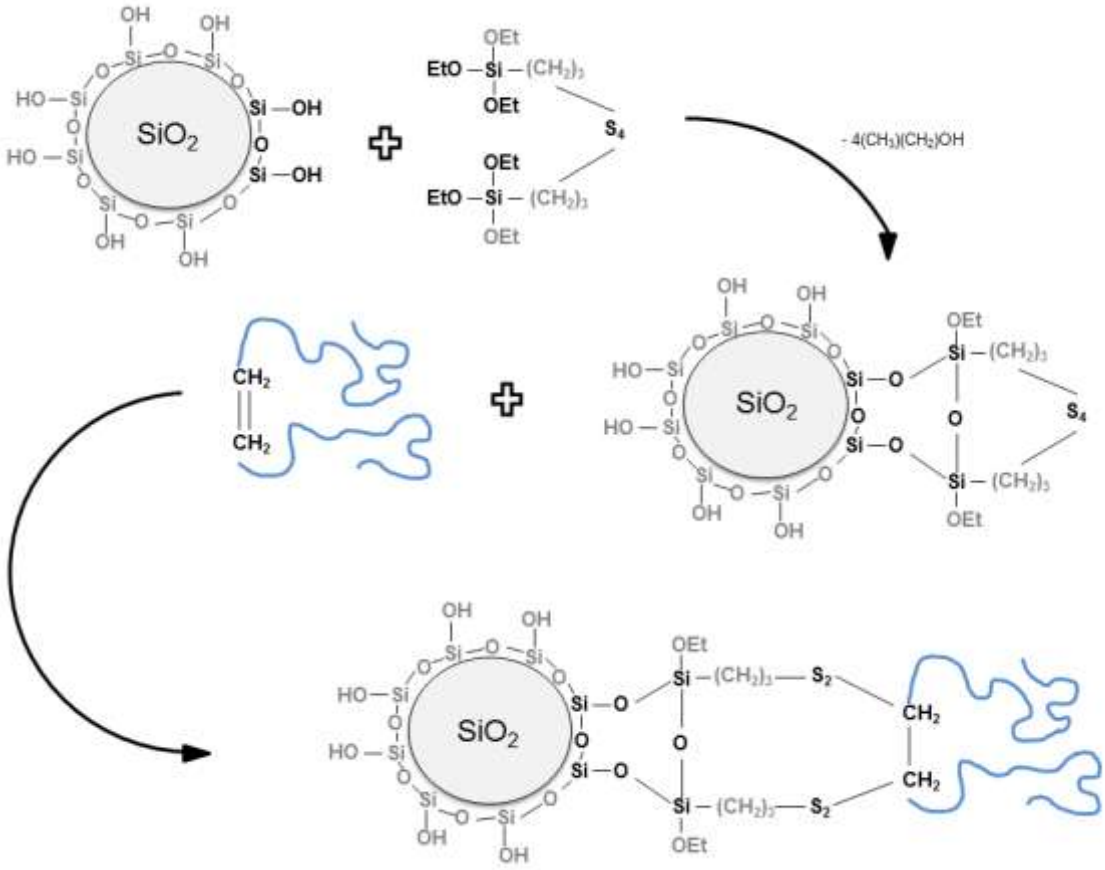

Fig. 4 – Schematic illustration of the reaction between silica, silane and rubber.

1.2.1 Preparation of Rubber Composites

The typical manufacturing sequence in rubber industries includes: mixing/compounding, forming and vulcanizing. Rubbers, fillers and the other additives (curing agents, protectors, plasticizers, process helper) are mixed together in two steps using two machines. In the first step, the materials are mixed in a close internal mixer, called Banbury, which includes two tangential rotors and a piston (Fig.5a). In the second step, the two-roll mill is used: this is an open machine with two horizontal and cylindrical rotors (Fig5b). Both machines are based on the sharing force generated by the rotors that rotate in opposite directions. The mixing is regulated by the speed, the temperature and size of the rotors, the mixing time and by the use of the piston, in the case of the internal mixing.

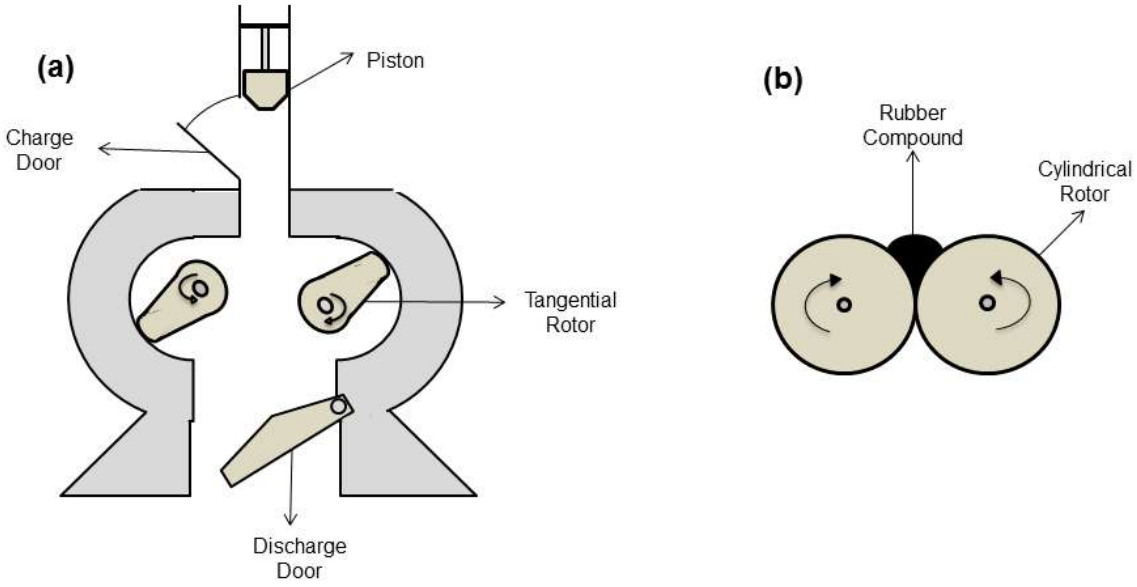

Fig. 5 – Schematic illustration of (a) internal mixer and (b) two-roll mill.

After mixing the compounded rubber becomes plastic and ready to be formed in an appropriate shape for the following vulcanization. In rubber industries screw-type extruders are used for this operation. For example, the extruder screw forces the rubber through a pair of rolls to form a slab or a sheet. Otherwise, the rubber compound can be used to coat textiles or steel cords in a calender. After the rubber compound has been processed and formed, it is vulcanized. In the most popular vulcanization method, the rubber compounds are cured at high temperature and pressure in a suitable mold. Other methods include heated dry air vulcanization and microwave vulcanization [1,3,12].

1.3 Rubber Nanocomposites

In recent years, researchers both in industry and universities have focused their interest on polymeric nanocomposites, which represent a radical alternative to conventional filled polymers [13]. In contrast to the conventional system, the reinforcement particles in the nanocomposites have at least one dimension in the nanometer size range (1-100 nm). The

advantage of using nanoscale fillers is that, if uniformly dispersed in matrices, they possess high interfacial area per unit volume and extremely short inter-filler distance. The higher surface area of the nanoparticles results in a high degree of adhesions with the polymeric chains. Hence, under loading, nanoparticles interact with each other and with the polymeric chains more efficiently than traditional filler, thus restraining the matrix molecular deformation [10]. Nanoparticles are characterized by high aspect ratios; consequently, their orientation in the matrix is another important factor in the reinforcement. They will restrain more the matrix deformation if they are aligned with the tensile stress direction [14]. The reinforcing effect of nanofiller depends on the geometrical characteristics and intrinsic properties of nanomaterials, the dispersion, concentration and orientation of the nanoparticles in the matrix, and on the interactions between elastomeric chains and the nanofiller [9]. These characteristics explain why nanofiller improve significantly the properties of elastomers (such as mechanical and gas barrier properties) already at low loading, leading to lightweight nanocomposites with lower cost.

Ever since Toyota presented layered silicates (LS)/polyamide nanocomposites in the early 90s [15], LS have been widely investigated as potential nanofiller for rubber nanocomposites. LS, also called clays, are two-dimensional nanoparticles and belong to layered silicate minerals or phyllosilicates. The fundamental building elements of clay are composed of 2D-sheets of silica and oxygen atoms arranged in a tetrahedral structure and 2D-sheets of aluminum and/or magnesium and oxygen atoms arranged in an octahedral structure. The individual sheets condense in discrete platelets, also called layers [16]. The ratio between the tetrahedral and octahedral sheets defines the clay: for example Montmorillonite (MMT), the most popular clay, has a ratio of 2:1 between the silicate and aluminum/magnesium sheets. Hence, in the MMT structure, the octahedral sheet is sandwiched between two tetrahedral sheets (Fig.6a). Usually, isomorphic substitutions within the layers (for example,

Al^{3+} replaced by Mg^{2+}, or Mg^{2+} replaced by Li^{+}) generate negative charges that are balanced by alkali cations. Thus, cations are situated in the interlayer space [17]. Each layer has a thickness of about 1 nm and a width from 30 nm to several μm; hence, a single layer present a high aspect ratio [18]. Usually, the layers arrange themselves into big stacks due to the Van der Walls force.

Naturally, the dispersion of inorganic nanofiller in an organic matrix like rubber is very difficult. This problem can be solved by modifying the interlayer space. When organic cations are added to water-clay dispersion, the alkali cations are replaced by long organic chain with positive charge [19-21]. Thus, the LS becomes more compatible with elastomeric matrix. Usually, alkyl ammonium ions are used to modify LS; they present the following basic formulas: $[R\text{-}NH_3^+]$, $[R_2\text{-}NH_2^+]$, $[R_3\text{-}NH_1^+]$ and $[R_4\text{-}N^+]$. The exchange of ions in the clay structure results also in the expansion of the interlayer distance (Fig. 6b). These modified clays are called organoclay [16].

Layered double hydroxides are positive charged LS; the interlayer space of LDHs contains exchangeable anions. Thus LDHs are also known as anionic clays. Their structure is very similar to the mineral brucite ($Mg(OH)_2$), in which each Mg^{2+} is octahedrally surrounded by six OH^-. The octahedrons share their edges to form a two-dimensional layer. The partial replacement of Mg^{2+} by trivalent cations results in the positive charged interlayer space. LDHs can be modified by organic anions (such as dodecyl sulfate), in order to be more easily dispersed in the polymers. Consequently, this anionic substitution results in an increase of the interlayer space [22].

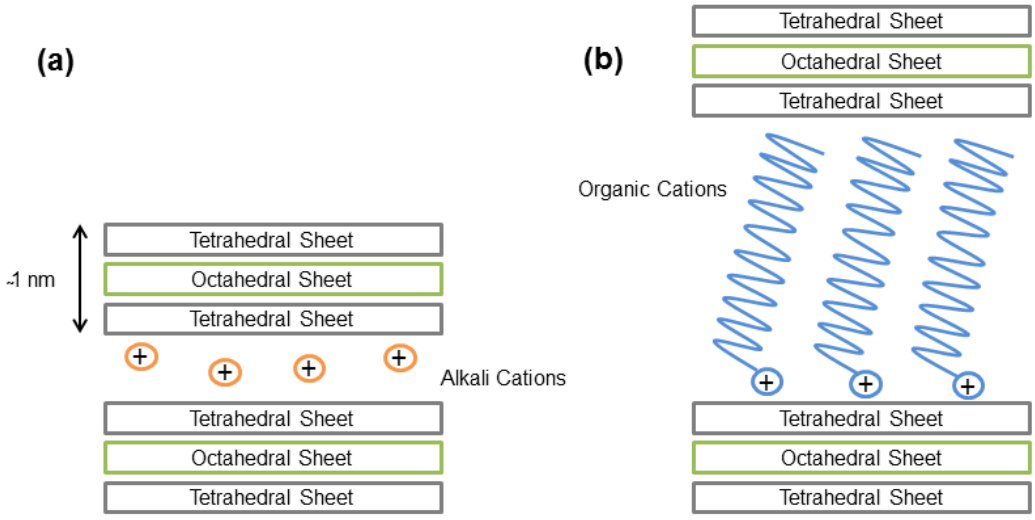

Fig. 6 – Scheme of (a) MMT and (b) organo-MMT.

Beyond LS, also carbon nanotubes (CNTs) have been largely used as nanofiller in polymer nanocomposites [23-25], since their discovery in 1991 [26]. CNTs are made of sp^2 carbon atoms arranged in a cylindrical structure with a diameter of a few nanometers (1-10 nm). As shown in Fig. 7, a CNT can be also visualized as a rolled graphene sheet. The length range goes from several micrometers to millimeters, or even centimeters [27]. Consequently, an individual CNT presents a very high aspect ratio and they are considered the one-dimensional allotrope of carbon. There are two basic type of CNT: single wall carbon nanotubes (SWCNTs), which are made of one individual cylinder (Fig. 10a); and multi wall carbon nanotubes (MWCNTs), which consist of concentric tubes (Fig. 10b) [28,29]. CNTs show outstanding mechanical properties and high thermal and electrical conductivity [30].

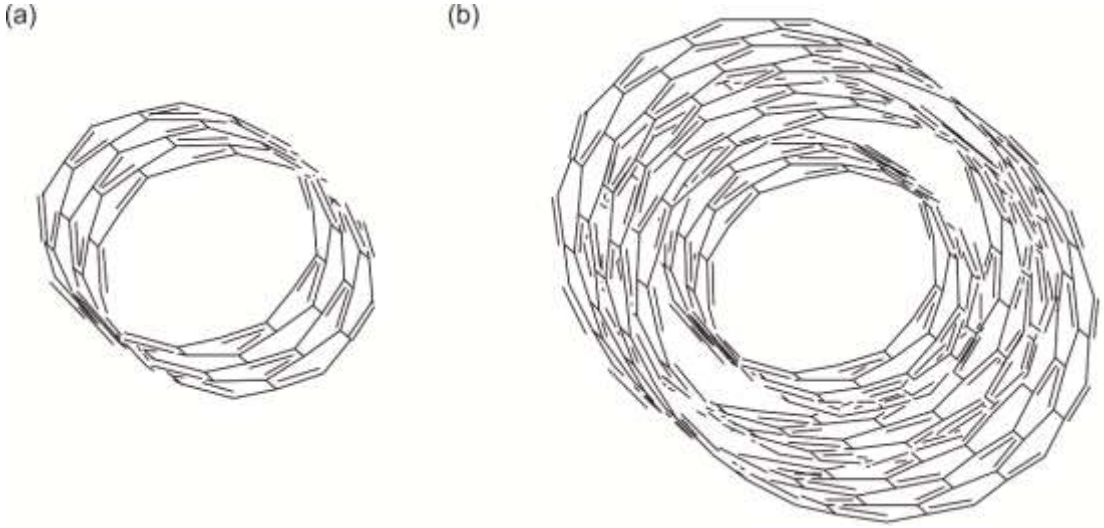

Fig. 7 – Representation of (a) SWCNT and (b) MWCNT.

CNTs are mainly synthetized with three different methods: arc-discharge, laser ablation, and catalytic vapor deposition (CCVD). In the arc discharge method, a current (50-100 A) is passed through two graphitic electrodes in an inert atmosphere and carbon atoms are vaporized from the positive electrode (anode) and deposited on the negative electrode (cathode). The deposit on the cathode contains CNTs and other carbons material, and because of this a further purification is necessary [31]. To obtain only SWCNTs, the graphitic electrodes are doped with metal atoms (nickel and cobalt) [32].

In laser ablation, a powerful laser is used to ablate a graphitic target, which contains small amount of metal atoms, in inert atmosphere at high temperature (1200 °C). The laser beam causes the evaporation of carbon atoms and a carrier gas sweeps the carbon atoms from the high temperature zone to a cold collector, where they condense into CNTs [33].

These two methods produce limited amount of CNTs but by using CCVD larger quantities of CNTs are obtained. A hydrocarbon source (methane, acetylene or ethylene) is heated at high temperature (500-1000 °C) in a quartz tube in presence of catalytic metal nanoparticles. The pyrolysis of the carbon source results in CNTs [34]. This is a low cost

method to produce large amount of CNTs and the morphology of CNTs is regulated by the catalyst system. For example, nanoparticles of iron and cobalt form the catalyst system for MWCNTs, whereas SWCNTs are synthetized in the presence of iron and molybdenum nanoparticles [32].

In addition to clays and CNTs, graphene and its derivatives have been widely analyzed and studied as nanofiller of elastomer nanocomposites [35]. Graphene consists of sp^2 carbon atoms arranged in an atomically thick honeycomb structure [36]. Graphene is the two dimensional allotrope of carbon and it is considered the building element of the carbon allotropes with different dimensionality (Fig. 8). Graphite, the three dimensional allotrope, consists of several graphene sheets stacked, bonded by π-π interactions and separate by 3.37 Å; CNTs (one dimensional) and fullerene (zero dimensional) are made by rolling and slicing graphene sheets, respectively [37].

In 2004 graphene was isolated for the first time from graphite through a process called micromechanical cleavage or scotch tape technique [38]. This nanoparticle presents extraordinary mechanical properties, such as Young's modulus of 1 TPa, tensile strength of 130 GPa [39], and has high thermal (5000 W/(m*K) [40] and electrical conductivities (6000 S/cm) [41]. Moreover, the surface area of graphene is about 2600 m^2/g. These properties, its gas impermeability [42] and the ability to be dispersed in polymeric matrices have created potential nanofiller for nanocomposites.

Fig. 8 – Graphene as a building element of the carbon allotropes with different dimensionality: fullerene, carbon nanotube, graphite [43].

Several routes have been explored to produce graphene, including "bottom-up" and "top-down" processes. In the "bottom-up" processes, carbon compounds are converted into graphene. Typical "bottom-up" processes are: chemical vapor deposition (CVD), reduction of CO, epitaxial growth on silicon carbide (SiC) and arc discharge [44]. CVD is the most popular. It is based on the conversion of carbon gases (methane, acetylene, or ethylene) and the growth of graphene occurs on a metal (copper or nickel) substrate [45]. The "bottom-up" processes produce defects of the free graphene layer but these processes are expensive and able to produce only a small amount of graphene [37].

"Top-down" processes are based on the exfoliation of the graphite and its derivatives [46]. They are schematically summarized in Fig. 9.

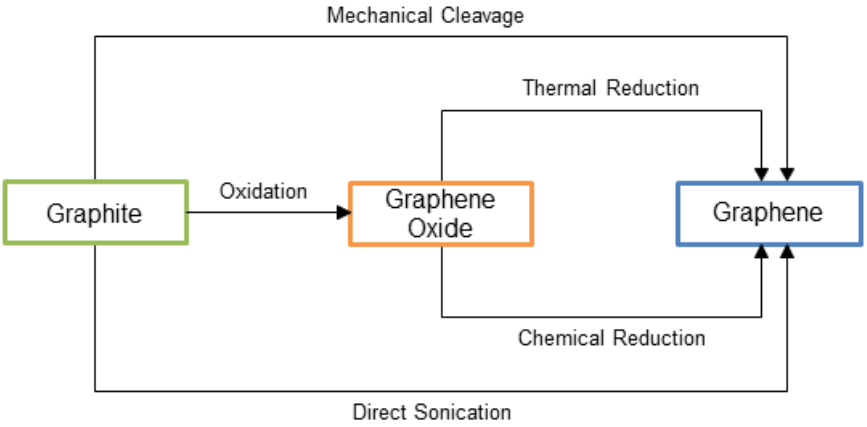

Fig. 9 – Top-down processes to produce graphene from graphite.

Mechanical exfoliation or cleavage is a relatively simple method to obtain graphene from graphite, but in very limited quantity [38]. Graphite has been directly exfoliated via sonication in the presence of polyvinylpyrrolidone [47] or N-methylpyrrolidone [48]. The weak point of this method is the separation of graphene sheets from the bulk of graphite.

Nowadays, the most promising method to produce graphene in large scale consists of two steps: in the first one, graphite is oxidized in in graphene oxide (GO) by strong oxidants (H_2O_2, $NaNO_2$, $KMnO_4$, and $KClO_3$) in presence of nitric and sulfuric acids. This phase lasts 10-12 hours and is supported by ultrasounds [44]. GO has a layered structure similar to that of graphite but the interlayer space is between 6 and 10 Å. Moreover, the surface of the GO sheets presents several functional groups: epoxide and hydroxyl on basal plane, and carbonyl and carboxylic at the edge [37]. Subsequently, in the second step, GO is reduced and exfoliated in graphene. GO can be reduced by chemical or thermal process. In the first route, hydrazine or hydroquinone is used as a reductant and the ultrasounds induce the exfoliation in graphene [13]. The cost and dangerous nature of the chemicals are the limit of this reduction method. In the thermal route, GO is reduced and exfoliated by rapidly heating (>2000 °C/min) in an inert atmosphere at high temperature (> 1000 °C). The absence of chemicals makes the

thermal reduction route the more convenient method to prepare graphene in large amounts [46]. The oxidation of graphite in GO and the following thermal reduction / exfoliation are shown in Fig. 10.

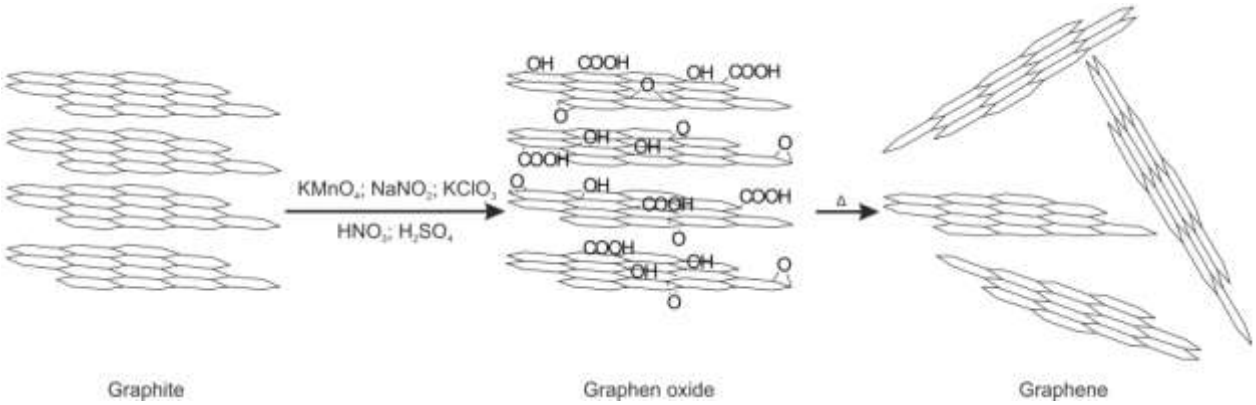

Fig. 10 – Preparation of graphene by means of oxidation and thermal reduction / exfoliation of graphite.

This method is also used to produce multilayer graphene (MLG), a nanoparticle made of 7-15 graphene sheets. MLG and GO can be used to reinforce polymer at low loading. The increase in the number of layers results in a reduction of the surface area and in the intrinsic properties of the graphene stacks compared to the single layer graphene. However, Gong *et al.* reported that monolayer graphene will not necessarily give the best reinforcement. Consequently, MLG is a good nanofiller despite its reduced intrinsic properties compared monolayer graphene [49,50].

Expanded graphite (EG) is another nanofiller derived from graphene and produced through the exfoliation of graphite. EG consists of 15-75 graphene sheets. The first step of the production of EG is the intercalation of graphite by sulfuric and nitric acids. The intercalation results in an increase of the interlayer space of graphite; this effect facilitates the successive

thermal exfoliation. The intercalated graphite is exfoliated into EG through a rapid heating at high temperature [51].

Recently, bionanofillers, such as polysaccharides and wood fibers, have been proposed as reinforcing nanomaterial for rubber nanocomposites because they are low cost biodegradable materials [52,53].

1.3.1 Preparation of Rubber Nanocomposites

The properties of rubber nanocomposites depend strongly on how well the nanofillers are dispersed in the elastomeric matrix. Nanoparticles tend to form aggregates; therefore their dispersion is not easy. Obviously, the dispersion of the nanofiller strongly depends on the preparation method of the nanocomposites. Thus, in the literature several preparation methods have been discussed. The most popular are: melt compounding, solution mixing, latex compounding, and in-situ polymerization [10,13].

The melt compounding is a direct way to mix elastomer, nanoparticles and the other ingredients (curatives, etc.) using mainly two machines (described in the previous sections): the internal mixer and the two-roll mill (Fig. 4). This method is the most cost effective and environmental friendly because solvents are not needed [54,55]; it is also completely compatible with rubber industry, where the two machines are usually employed. Nevertheless, the melt compounding procedure often doesn't guarantee a good dispersion of nanofillers [56-58]. Moreover, the handling and the milling of the nanoparticles with traditional machines are not easy. For example, an inappropriate handling of nanofillers on the two-roll mills will result in a small cloud of nanoparticles dispersed in the air.

In contrast, the other three methods are not direct because they include the preparation of a masterbatch (Fig. 11), which consists of only rubber and nanofiller. Successively, the

masterbatch is mixed together with the other ingredients of the rubber nanocomposites in the typical machines of the rubber manufacturing (internal mixer or in the two roll mill). The masterbatch simplifies tremendously the handling of the nanoparticles because it is a solid ingredient that can be easily added in the two-roll mill or the internal mixer. Unfortunately, a suitable solvent is necessary in the solution mixing, the latex compounding, and the in-situ polymerization.

and in situ polymerization, in the case of layered nanofiller.

In the solution mixing the solvent should be able to dissolve the rubber and suspend the nanofiller. The most common solvents are toluene, tetrahydrofuran and dimethylformammide. The rubber solution and the suspension of the nanofiller are mixed together using mechanical stirring and ultrasounds. Usually, the sonication improves the dispersion of the nanoparticles because the ultrasound waves break the aggregates of the nanofiller. The masterbatch is obtained after the evaporation of the solvent. Alternatively, the masterbatch is coagulated by adding another solvent. Although the solution mixing is not an environmental friendly method to prepare rubber nanocomposites because organic solvents are necessary, it is very popular because it provides a good dispersion of the nanofiller [59-63].

In the latex compounding the solvent is water. Some common rubbers are commercially available in the latex form: this consists of fine elastomers particles dispersed in water. Hence, in this method nanofillers are mixed with rubbers in latex form by means of mechanical stirring and sonication. The mixture is then coagulated and the masterbatch is dried. Latex compounding yields to good dispersion of the nanofiller in an environmental friendly way because of the use of water; this is biggest advantage of this method [64,65]. Unfortunately, not all rubbers are available in the latex form.

In the in-situ polymerization method, the nanofiller is mixed and dispersed in a solution of a monomer or multiple monomers. After the polymerization of the rubber, the masterbatch is obtained through the evaporation of the solvent or its coagulation, like in the solution mixing. Also this method guarantees a good dispersion of the nanofiller, but it is clearly the most complicated one because of the occurring of the polymerization. Moreover, the employment of organic solvents and others chemicals (monomers, catalysts, etc.) makes the in-situ polymerization an expensive and not environmental friendly method to prepare nanocomposite [66-68].

Similarly to rubber composites, after mixing, rubber nanocomposites are suitably formed and vulcanized at high temperature and high pressure.

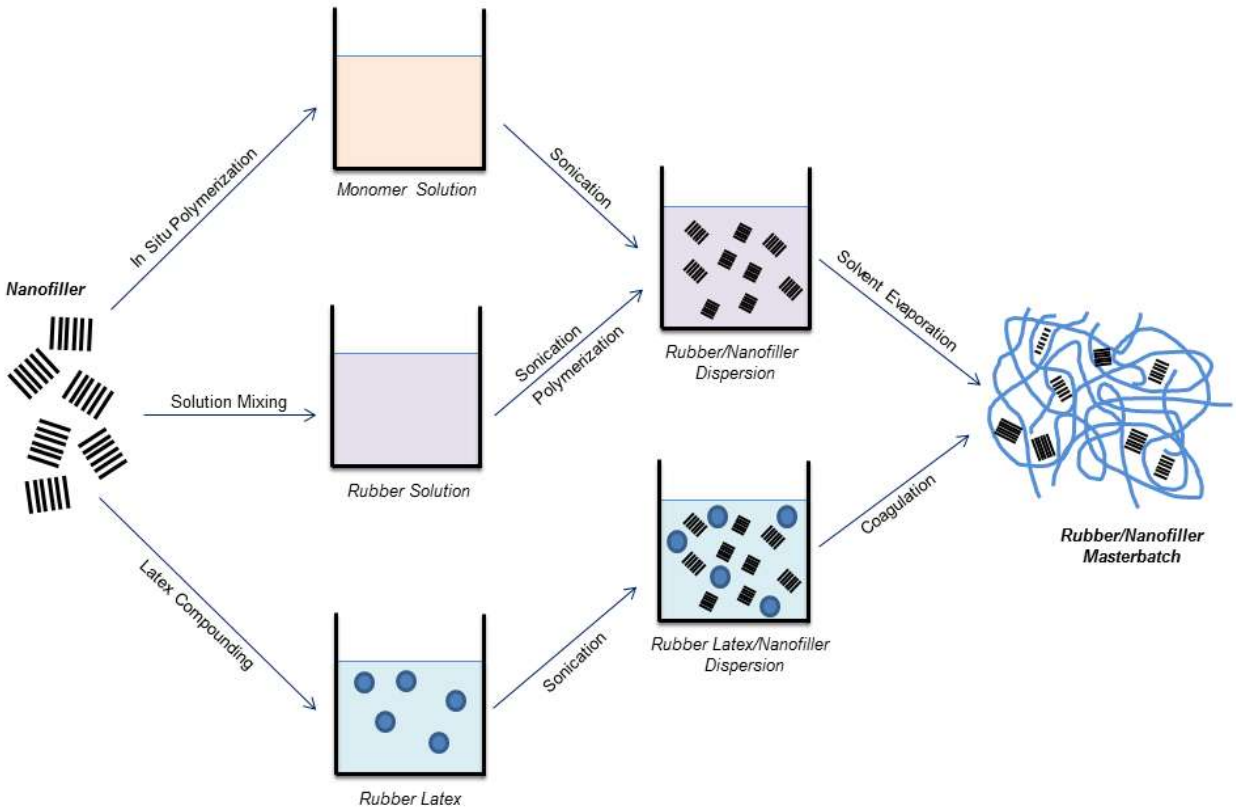

Fig. 11 – Preparation of rubber/nanofiller masterbatch using solution mixing, latex compounding

2. Scientific Goal

High loading (>40 phr) of CB or silica are usually used to achieve the requested mechanical and functional properties of rubber composites. In recent years several nanoparticles (such as LSs, CNTs, EG and graphene) have been proposed as nanofiller for elastomer nanocomposites. When incorporated appropriately, these nanoparticles can significantly improve the mechanical and functional properties (hardness, modulus, gas barrier properties) of the rubbers at extremely small loading.

In this study the multifunctional impact of the MLG on the different properties (curing, rheological, mechanical and functional) of the unvulcanized and vulcanized rubbers nanocomposites is largely investigated. Thus MLG is proposed as an efficient nanofiller for rubbers, in order to improve the overall performances of unfilled rubbers and rubber/CB composites, and also to reduce the filler content. MLG is a nanoparticle made of just approximately 10 graphene sheets and has recently become commercially available for mass-product nanocomposites.

The reinforcement effect of the nanofiller depends on several factors: intrinsic properties, geometric parameters of the nanofiller, the dispersion and the concentrations of the nanofiller in the elastomeric matrix and the interactions between polymeric chains and the nanofiller. In order to investigate the reinforcing effect of the tested nanoparticles, systematic comparisons between unfilled rubbers and nanocomposites prepared through different methods, nanocomposites with different MLG content, nanocomposites based on different rubbers, respectively, are studied.

The efficiency of MLG is determined by means of a multi-methodic comprehensive characterization: curing and rheological properties of the uncured rubber nanocomposites; a large variety of mechanical properties and different functional properties (gas barrier and flame retardant properties, electrical and thermal conductivities) of the cured nanocomposites.

The characterization includes also the morphological analysis of the surface of the nanocomposites. Moreover the protective effect, against the weathering aging, of MLG is studied and illustrated.

In the first paper the effect of the preparation method and hence of the nanofiller dispersion on the properties of the rubber nanocomposites is investigated. CIIR/MLG nanocomposites with the same MLG content (3 phr) were prepared directly on a two-roll mill (melt compounding) and by pre-mixing MLG with CIIR using an ultrasonically-assisted solution mixing procedure followed by two-roll milling, in order to evaluate the effectiveness of these different preparation methods.

Since the solution mixing provided a homogeneous dispersion of the MLG and hence nanocomposite with the better properties, this method was used for the following investigations. The concentration of the nanofiller is another crucial parameter in the reinforcement of rubber nanocomposites. Therefore, in the second paper, CIIR/MLG nanocomposites with different MLG loadings are characterized in order to determine the effect of the nanofiller concentration on the properties of the nanocomposites.

The chemical structure of the rubber and hence the interactions between elastomeric chains and nanofiller play an important role in the reinforcement of rubber nanocomposites. Thus nanocomposites with different rubbers and the same loading of MLG (3 phr) are characterized in the third paper in order to understand the effect of the rubber/nanofiller interactions on the properties of nanocomposites. The investigated rubbers are: CIIR, NBR, NR and SBR. These elastomers are usually employees in multi sector applications, such us tires, gloves, shoes and seals.

In the last paper of this study, 3 phr of MLG were added to CIIR/CB composites in order to partly replace CB or to improve performance, respectively. The combination of

nanoparticles and traditional fillers is a reasonable approach to exploit nanocomposites in the usual industrial applications.

3. Publications and Manuscripts

3.1 Multilayer Graphene / Chlorine – Isobutene – Isoprene Rubber Nanocomposites: The Effect of Dispersion

Daniele Frasca, Dietmar Schulze, Volker Wachtendorf, Michael Morys and Bernhard Schartel, *Polym. Adv. Technol.* **2016**, 27 (7), 872-881.

This article was published.

http://dx.doi.org/10.1002/pat.3740

Author Contribution:

- Designing the working packages and the approach to this study;
- Masterbatches, rubber compounds and samples preparation;
- Experiments for rheological, curing and mechanical properties;
- Experiments for electrical conductivities;
- Data evaluation;
- Manuscript Preparation;

3.2 Multilayer Graphene (MLG) Chlorine Isobutyl Isoprene Rubber Nanocomposites: Influence of the MLG-Concentration on Physical and Flame Retardant Properties

Daniele Frasca, Dietmar Schulze, Martin Böhning, Bernd Krafft and Bernhard Schartel, *Rubber Chem. Technol.* **2016**, 89 (2), 316-344.

This article was published.

http://dx.doi.org/10.5254/rct.15.84838

Author Contribution:

- Designing the working packages and the approach to this study;
- Masterbatches, rubber compounds and samples preparation;
- Experiments for rheological, curing and mechanical properties;
- Experiments for electrical conductivities;
- Data evaluation;
- Manuscript Preparation;

3.3 Multifunctional multilayer graphene / elastomer nanocomposites

Daniele Frasca, Dietmar Schulze, Volker Wachtendorf, Christian Huth and Bernhard Schartel, *Eur. Polym. J.* **2015**, 71, 99-113.

This article was published.

http://dx.doi.org/10.1016/j.eurpolymj.2015.07.050

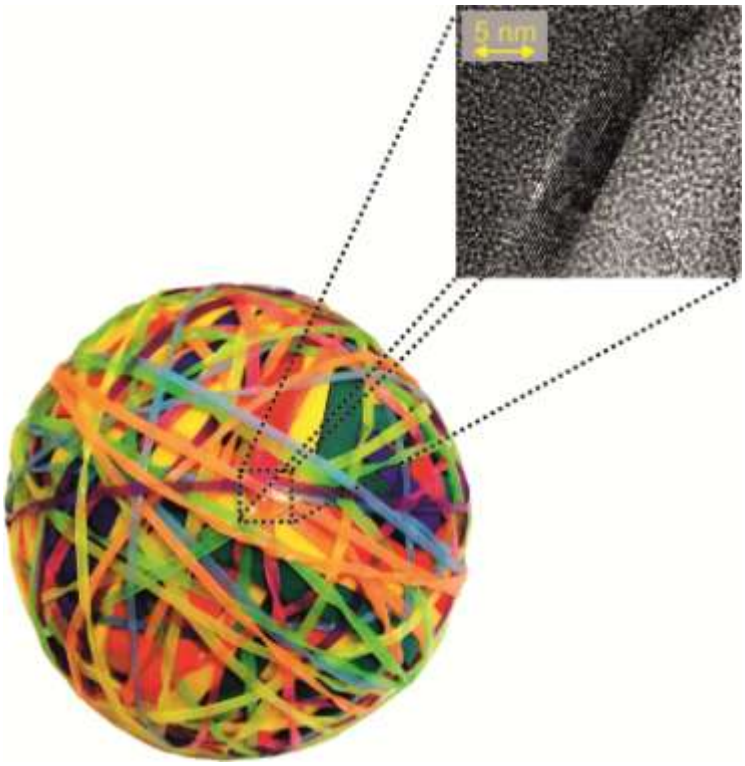

Author Contribution:

- Designing the working packages and the approach to this study;
- Masterbatches, rubber compounds and samples preparation;
- Experiments for rheological, curing and mechanical properties;
- Experiments for UV-Vis Absorbtions;
- Data evaluation;
- Manuscript Preparation;

3.4 Multilayer Graphene/Carbon Black/Chlorine Isobutyl Isoprene Rubber Nanocomposites

Daniele Frasca, Dietmar Schulze, Volker Wachtendorf, Bernd Krafft, Thomas Rybak and Bernhard Schartel, *Polymers* **2016**, 8 (3), 95

This article was published.

http://dx.doi.org/10.3390/polym8030095

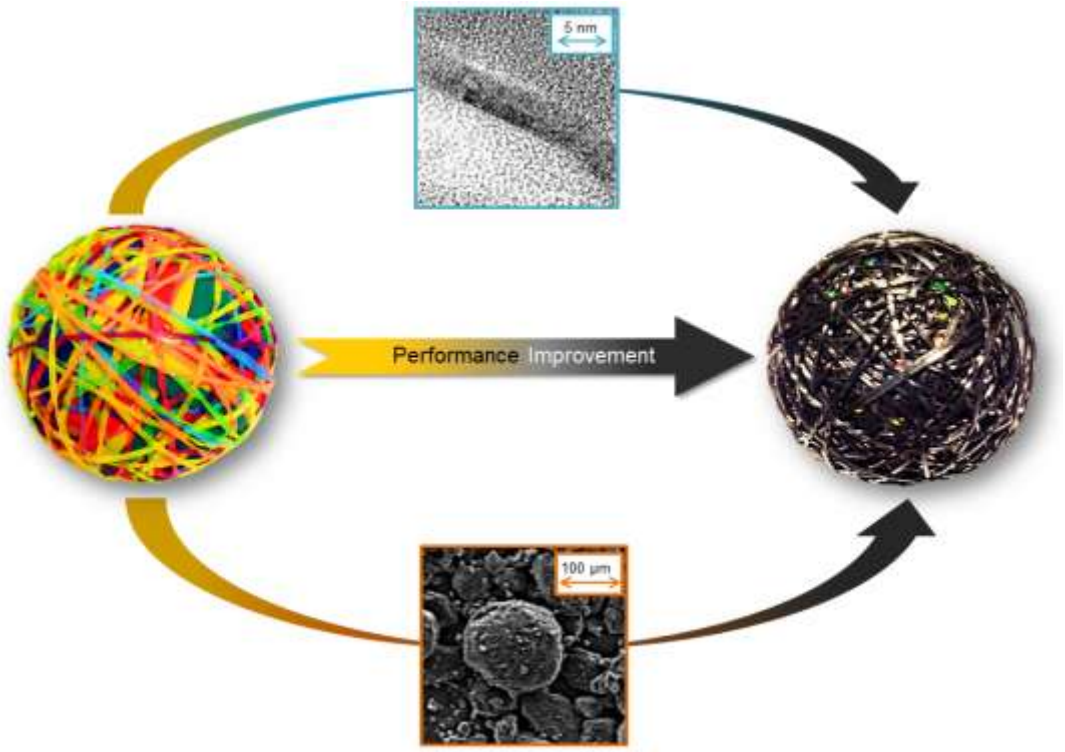

Author Contribution:

- Designing the working packages and the approach to this study;
- Masterbatches, rubber compounds and samples preparation;
- Experiments for rheological, curing and mechanical properties;
- Experiments for UV-Vis Absorptions;
- Data evaluation;
- Manuscript Preparation;

polymers

MDPI

Article

Multilayer Graphene/Carbon Black/Chlorine Isobutyl Isoprene Rubber Nanocomposites

Daniele Frasca, Dietmar Schulze, Volker Wachtendorf, Bernd Krafft, Thomas Rybak and Bernhard Schartel *

Bundesanstalt für Materialforschung und–prüfung (BAM), Unter den Eichen 87, 12205 Berlin, Germany; daniele.frasca@bam.de (D.F.); dietmar.schulze@bam.de (D.S.); volker.wachtendorf@bam.de (V.W.); bernd.krafft@bam.de (B.K.); thomas.rybak@bam.de (T.R.)

* Correspondence: bernhard.schartel@bam.de; Tel.: +49-30-8104-1021

Academic Editor: Walter Remo Caseri

Received: 10 February 2016; Accepted: 14 March 2016; Published: 22 March 2016

Abstract: High loadings of carbon black (CB) are usually used to achieve the properties demanded of rubber compounds. In recent years, distinct nanoparticles have been investigated to replace CB in whole or in part, in order to reduce the necessary filler content or to improve performance. Multilayer graphene (MLG) is a nanoparticle made of just 10 graphene sheets and has recently become commercially available for mass-product nanocomposites. Three phr (part for hundred rubbers) of MLG are added to chlorine isobutyl isoprene rubber (CIIR)/CB composites in order to replace part of the CB. The incorporation of just 3 phr MLG triples the Young's modulus of CIIR; the same effect is obtained with 20 phr CB. The simultaneous presence of three MLG and CB also delivers remarkable properties, e.g. adding three MLG and 20 phr CB increased the hardness as much as adding 40 phr CB. A comprehensive study is presented, showing the influence on a variety of mechanical properties. The potential of the MLG/CB combination is illustrated to reduce the filler content or to boost performance, respectively. Apart from the remarkable mechanical properties, the CIIR/CB/MLG nanocomposites showed an increase in weathering resistance.

Keywords: nanocomposites; rubber; multilayer graphene; carbon black

1. Introduction

Carbon black (CB) is largely used as filler to improve the performance of rubber composites. CB is produced by the partial combustion or thermal cracking of heavy petroleum products or natural gas. The fine particles of CB always form aggregates and agglomerates [1] and high filler loadings (>30 phr) are usually needed to obtain the mechanical performance desired for elastomer composites [2,3].

Ever since Toyota presented layered silicate/polyamide nanocomposites in the early 1990s [4], polymer research has been concentrating on nanocomposites, and several nanoparticles have been used to reinforce rubbers at even low concentrations. Typical nanofillers include: layered silicates [5,6], spherical nanosilica [7,8], carbon nanotubes [9,10], organically modified clay [11–13] and bionanofillers [14,15]. The discovery of graphene [16] has created a new potential nanofiller for polymer nanocomposites [17,18]. Graphene is the 2-D carbon allotrope consisting of a sheet of sp2 carbon atoms arranged in a honeycomb structure [19].

In this study, multilayer graphene (MLG) was used as a nanofiller. It presents a large specific surface area BET (Brunauer Emmett Teller): 250 m^2/g. This parameter describes quite well the degree of exfoliation and thus the number of layers in graphene stacks [20,21]. A single graphene sheet has a BET of about 2600 m^2/g. Therefore the MLG used is composed of approximately 10 graphene sheets. Recently, MLG has become commercially available at a reasonable price by applying a modified Hummer method. Materials with a specific surface area BET between 80 and 200 m^2/g and then stacks

consisting of more than 15 sheets are frequently referred to as graphene in the literature. However, we would like to use the following denotation: graphene (less than 7 layers), MLG (7–15 layers) and expanded graphite (15–75 layers) [22–25]. Even low loadings of MLG already reinforce the final properties of rubber nanocomposites [26,27].

The rubber tested was chlorine isobutyl isoprene rubber (CIIR), the chlorinated form of isobutylene isoprene rubber (IIR), or butyl rubber for short. It is a copolymer of isobutylene (97%–98%) and a small amount of isoprene (2%–3%). CIIR was developed to increase the curing rate of IIR, allowing contemporary vulcanization with natural rubber and styrene-butadiene rubber. Because CIIR presents a very airtight structure, it is the most important rubber for the inner linings of tubeless tires today [28].

The combination of nanoparticles and traditional fillers is a reasonable approach to exploit nanocomposites in usual industrial applications. Thus, in this study, 3 phr of MLG were added to CIIR/CB composites in order to replace CB in part or to boost performance, respectively. The CB used has a specific surface area BET between 70 and 100 m^2/g. The CIIR/CB compounds were prepared by melt-compounding using a two-roll mill. The compounds with MLG were prepared by pre-mixing MLG with CIIR by an ultrasonically-assisted solution mixing procedure followed by two-roll milling [29].

A low loading of 3 phr MLG was used and its significant influence on the rheological, curing and mechanical properties of CIIR and CIIR/CB composites investigated. Improvements were found, such as the increase in Young's modulus by a factor of 3 and the replacement of 20 phr CB.

Rubbers are very sensitive to weathering exposure: the combination of oxidative gases and UV degrades the elastomer matrix through multi-step photo-oxidation [30]. The UV absorption and radical scavenging of both CB and MLG was addressed and the improved weathering resistance of the CIIR/CB/MLG nanocomposites discussed.

2. Materials and Methods

2.1. Materials

CIIR (Chlorobutyl 1240), zinc oxide (Zincoxyd Activ), and mercaptobenzthiazole disulfide (MBTS, Vulcacit DM/C-MG) were obtained from LANXESS Deutschland GmbH, Leverkusen, Germany. Commercially available MLG (EXG R98 250) was produced by Graphit Kropfmühl AG, Hauzenberg, Germany. CB660 (CXN660) and CB (CXN330) were supplied by Orion Engineered Carbons GmbH, Frankfurt, Germany. Stearic acid (stearic acid pure) was produced by Applichem, Darmstadt, Germany. Sulfur was obtained from Merck, Germany. Struktol (Struktol 40 MS Flakes) was supplied by Schill + Seilacher, Böbligen, Germany. Analytical-degree toluene was obtained from Fisher Chemical, Schwerte, Germany.

2.2. Preparation of the CIIR Compounds

MLG was dispersed in a toluene/CIIR solution using a sonicator (UPS 400S, Hielscher, Teltow, Germany) for 3 h. Then the mixture was stirred for 2 h. The ratio of elastomer to MLG was 7:1 and the concentration of MLG in the solution was 1 mg/mL. The master batch was obtained after evaporation of the solvent (60 °C, 150 mbar) using a rotary evaporator (Hei Vap Value, Hiedolph, Schwabach, Germany).

CIIR and the other ingredients, as listed in Table 1, were mixed directly in a two-roll mill (Lab Walzwerk MT 6″ × 13″, Rubicon, Halle, Germany). The compounds were prepared in three stages. In the first stage, CIIR was mixed with zinc oxide, stearic acid, CB660 and Struktol. In the second stage, the CIIR/MLG master batch or CB was added to the rubber compound. In the third stage, the curatives (sulfur and MBTS) were added. For the compounds without MLG and CB, the second stage was not performed. For all compounds, the rolls were set to a temperature of 50 °C, a speed of 19 RPM a friction ratio of 1.1:1 and a mixing time of 20 min.

Table 1. Formulation of the CIIR (chlorine isobutyl isoprene rubber) compounds in parts per hundred of rubber (phr).

Ingredients	CIIR	CIIR/MLG3	CIIR/CB20	CIIR/CB20/MLG3	CIIR/CB30	CIIR/CB30/MLG3	CIIR/CB40
CIIR	100	100	100	100	100	100	100
Zinc oxide	3.0	3.0	3.0	3.0	3.0	3.0	3.0
Stearic acid	2.0	2.0	2.0	2.0	2.0	2.0	2.0
CB660	0.5	0.5	0.5	0.5	0.5	0.5	0.5
Struktol	7.0	7.0	7.0	7.0	7.0	7.0	7.0
Sulfur	0.5	0.5	0.5	0.5	0.5	0.5	0.5
MBTS	1.5	1.5	1.5	1.5	1.5	1.5	1.5
CB	-	-	20	20	30	30	40
MLG	-	3	-	3	-	3	-

The curing time (t100) was obtained by Dynamic Moving Die Rheometer (D-MDR 300, Montech Werkstoffprüfmaschinen, Buchen, Germany). It was 20 min for samples of 2-mm thickness and 25 for 6-mm thickness; the samples were vulcanized at a pressure of 300 bar and a temperature of 180 °C.

2.3. Characterization

UV-Vis absorption of freshly produced aqueous dispersions of CB (0.010 and 0.015 mg/mL), MLG (0.005 mg/mL) and their mixture (CB = 0.010 mg/mL plus MLG = 0.005 mg/mL) were measured with a Cary 300 Scan (Varian, Sidney (New South Wales), Australia) double monochromator double channel spectrometer in quartz cuvettes. For the measurement, the cuvettes were placed in front of a LabSphere® DRA-30I integrating sphere, which was used as samples producing stray light were investigated. The wavelength range was 800 to 220 nm with a step width 1 nm. MLG and CB were sonicated in water for 2 h. A baseline correction was carried out using a cuvette filled with pure water.

The radical oxidation of cumene (10 mL) was performed to determine the radical scavenging behavior of the tested carbon particles; AIBN (10 mg) was the initiator [31]. The studied reaction consists of 3 phases:

Initiation: AIBN → $r^{\bullet}$ + RH → $R^{\bullet}$
Propagation: $R^{\bullet}$ + O_2 → $RO_2^{\bullet}$ + RH → ROOH + $R^{\bullet}$
Termination: 2 $RO_2^{\bullet}$ → inactive products
(RH = cumene, $R^{\bullet}$ = cumylalkyl radical, $RO2^{\bullet}$ = cumylperxoy radical, ROOH = cumylhydroperoxide).

At 60 °C, the initiator (AIBN) decomposed into radicals (initiation). Then, the radicals reacted with cumene. This reaction resulted in cumene alkyl radicals, which were oxidized by oxygen into cumylperxoy radicals in the propagation stage. Furthermore, cumylperxoy radicals reacted with cumene, forming other cumene alkyl radicals. When cumylperoxy radicals reacted with each other, the reaction ended (termination).

MLG (5 mg, 30 mg) and CB (30 mg) were sonicated 10 minutes in the cumene. Than AIBN was added to the MLG/cumene dispersion and the oxygen consumption was controlled by measuring the pressure decrease in the closed air volume above the reaction mixture.

Using a Dynamic Moving Die Rheometer (D-MDR 3000, Montech Werkstoffprüfmaschinen), the dynamic viscosity (η') of the uncured samples (5 g) was measured as a function of frequency. The temperature was 100 °C and the strain amplitude was 1%. The storage modulus (G') as a function of the amplitude was also measured with a Dynamic Moving Die Rheometer (D-MDR 3000, Montech Werkstoffprüfmaschinen) on the uncured samples (5 g). The temperature was 60 °C and the frequency 1 Hz.

Scanning electron microscopy (SEM) micrographs of the freeze-fractured gold-coated surfaces of vulcanized samples were taken with a scanning electron microscope (Zeiss EVO MA 10) using an acceleration voltage of 10 kV. The micrographs of CB and MLG were taken without gold sputtering.

The samples (80 nm thick), for the TEM micrographs were prepared using a cryo microtome (Ultracut UCT, Leica, Wetzlar, Germany) at −100 °C. The TEM micrographs of CIIR-MLG-3 were taken with JEM-2200 FS (Jeol, Peabody, MA, USA); the acceleration voltage was 200 kV.

Tensile tests were performed on 5 dumbbell specimens (2-mm thickness) according to DIN 53504; Young's modulus tests were performed on 3 dumbbell specimens (2-mm thickness) according to ISO 527; and shore A hardness measurements were performed according to ISO 7619-1 on 3 samples of 6-mm thickness.

The storage modulus (G′) and dynamic loss factor (tan δ) were measured on 2 samples of 2-mm thickness as a function of temperature using an MCR 501 Rheometer (Anton Paar, Ostfildern, Germany). The frequency was 1 Hz, the strain amplitude was 0.1%, the temperature range of −80 to 70 °C and the heating rate was 1 °C/min.

The weathering/ageing process of dumbbell 10 test specimens (2 mm thickness) was conducted using the 24 h weathering cycle in Table 2 repeatedly conducted over 1000 h (for one half of the samples) and 1500 h (for the other half), respectively. The conditions of the cycle contain a step at −10 °C, which could bring mechanical tension into the sample, as well as rain phases, which can cause extraction of soluble or dispersible components off the system. Weathering was carried out using a fluorescent UV lamp device of the type Global UV Test 200 (Weiss Umwelttechnik GmbH, Reiskirchen, Germany), according to ISO 4892-3. The spectral distribution—characterized by UVA-340 nm fluorescent lamps (ISO 4892-3, type 1A) and spectrally neutral filtering using a PVDF-membrane in the device's door—was measured in the sample plane by means of a MSS 2040 spectro-radiometer. As the spectral distribution from the fluorescent lamps is limited to UV and near VIS, radiation heating can be neglected (TSurface − TChamber < 2 K). Thus, the degradation-relevant temperature can be controlled very closely over a wide range. The device allows full humidity control and uses water spraying for the wetting phases. UV-irradiance was 40 W/m^2.

Table 2. Weathering exposure cycle. Continuous UV irradiation at 40 W/m^2.

Time/h	Temperature/°C	Humidity
4	25	Rain
4	80	<10%
4	25	Rain
4	80	<10%
4	25	Rain
4	−10	<10%

3. Results

3.1. Characterization of MLG and CB

The left side of Figure 1 shows the SEM micrographs of the MLG used. The MLG particles had different shapes, but most of them present a worm-like shape (Figure 1a). Some particles are small with a diameter about 50 µm and others very big with a length of about 1 mm. Nevertheless, each particle consists of several MLG stacks (Figure 1b). Figure 1c shows the highly delaminated structure of MLG, in good correspondence to the high BET.

The SEM micrographs of CB are shown in the right side of Figure 1. The CB particles presented a spherical shape with diameters between 20 and 100 µm. Furthermore, the surface of the particles turns out to be completely smooth. At this magnification, no aggregates of CB particles were observed.

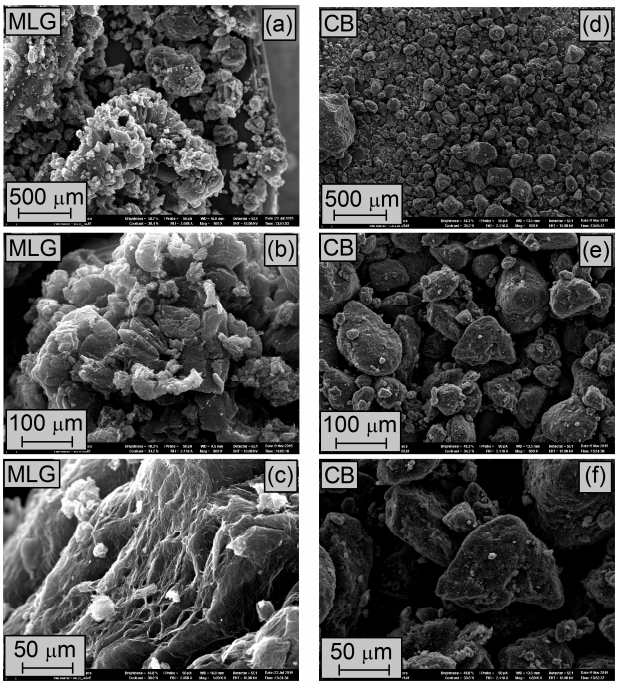

Figure 1. SEM micrographs of (**a**–**c**) MLG and (**d**–**f**) CB.

Figure 2 reports the UV-Vis absorption of aqueous dispersions of CB, MLG and a mixture of the two carbon particles. All of the spectra presented a maximum of absorption of about 270 nm, which corresponds to the electronic transition from the bonding orbital π to the anti-bonding orbital π^* [32]. This transition is typical for carbon particles like MLG and CB [33]. The UV band of the π-π^* transition is more defined in the spectrum of MLG (0.005 mg/mL), where it is almost a peak, than in the spectra of CB (0.010 and 0.015 mg/mL), where it is large and rough . MLG consists of only sp2 carbon atoms, whereas CB is made of sp2 and sp3 carbon atoms; in the presence of sp3 carbon atoms the UV band caused by π-π^* transition is reduced [34]. The spectra of the CB/MLG mixture presented an evident peak at about 270 nm because of the presence of the tested nanoparticle. Moreover, the absorption of the mixture, with a final concentration of 0.015 mg/mL, was higher than for the same concentration of CB. Hence, MLG presented a higher UV-Vis. absorption than CB.

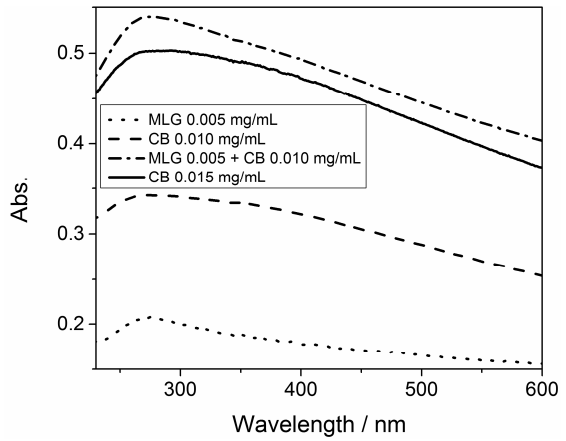

Figure 2. UV-Vis absorption of water dispersions of CB, MLG and their mixture.

The radical scavenging efficiency of the CB and MLG was determined by studying the radical oxidation of cumene [35], which is thought to be a model for autoxidative radical oxidation of the

elastomer. When this reaction occurs, it consumes oxygen, which results in a reduction of the pressure, as shown in Figure 3. The reaction started in a few minutes without MLG and CB. In the presence of CB and MLG, the reaction started after an induction time: 11 min for MLG and 13 min for CB, with the induction time as a parameter of the stabilization present in the system. The concentration of MLG was 0.5 mg/mL, while the concentration of CB was six times higher (3 mg/mL). The two carbon particles inhibited the oxidation of cumene because they intercepted the cumene alkyl radicals. Moreover, after the induction time, the pressure reduced more slowly in the presence of MLG than with CB. The radical scavenging efficiency of MLG increased with the concentration of the nanoparticle. The induction time with a concentration of 3 mg/mL of MLG was about 50 min.

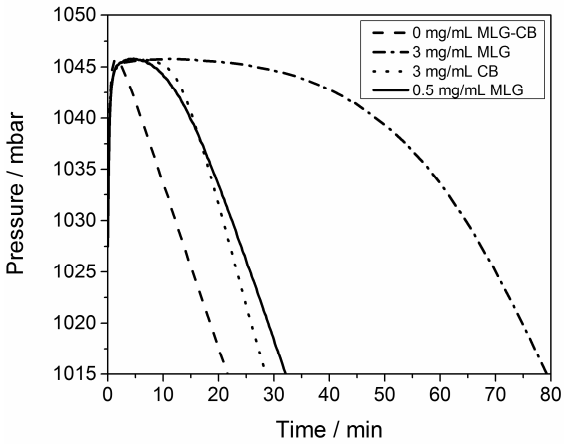

Figure 3. Change in pressure during the cumene oxidation with and without MLG or CB.

MLG was more efficient than CB because of its larger surface area and its chemical structure made only of sp2 carbon atoms. In this hybridization the carbon atoms have a free π orbital. The electrons of the radicals were delocalized in the free π orbital of MLG. The carbon atoms of carbon black present sp2 and sp3 hybridization, and thus fewer free π orbitals than MLG.

3.2. Rheological Properties of the Uncured Systems

Figure 4a shows the dynamic viscosity (η′) of the uncured systems as a function of the frequency. The frequency sweep shows a decrease in η′ for higher frequencies, because the elastic behaviour loses importance. CB and MLG reinforced CIIR in terms of η, as reported by Kumar *et al.* [36]; in fact, the curves of the filled systems show a remarkable shift to higher values in the logarithmic presentation compared to CIIR.

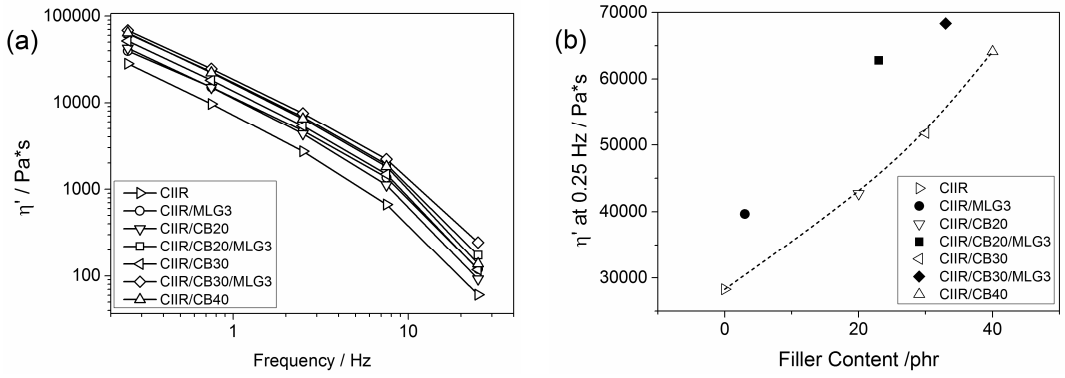

Figure 4. (**a**) Dynamic viscosity as a function of the frequency of CIIR and its composites; and (**b**) dynamic viscosity at 0.25 Hz as a function of the filler content; the line is a visual guide.

In Figure 4b, the η′ at 0.25 Hz is plotted as a function of the filler content. The reinforcement of 3 phr MLG in η′ corresponded to the reinforcement of more than 10 kPas and thus to an equivalent of 18 phr CB. The viscosity η′ increased with CB content: 20, 30 and 40 phr of CB resulted in reinforcing effects of 34%, 45% and 56%, respectively. The reinforcing effect of CB was increased by MLG. The combination of 20 phr CB and 3 phr MLG increased η′ by around 20 kPas and thus like 39 phr CB; hence, in this case, 3 phr MLG replaced 19 phr CB. The value of η′ at 0.25 Hz of CIIR/CB30/MLG3 was the highest and equal to that for 46 phr CB. As to the effect on η′, 3 phr MLG replaced at least 15 phr CB in CIIR/MLG/CB nanocomposites. The efficiency of the nanofiller was somewhat higher in combination with a low CB loading.

Figure 5a shows the G′ of the uncured systems as a function of the strain amplitude. Usually, the G′ values of unfilled rubber systems do not change along with amplitude. For the filled system, G′ increases with the decreasing amplitude because of the formation of a filler network [37]. This behaviour of filled rubber systems is known as the "Payne effect". In fact, no "Payne effect" was observed for CIIR and it was small for CIIR/MLG3, CIIR/CB20 and CIIR/CB30. The "Payne effect" becomes evident at higher filler loadings, as reported by Fritzsche *et al.* [38], and hence for CIIR/CB20/MLG3, CIIR/CB30/MLG3 and CIIR/CB40.

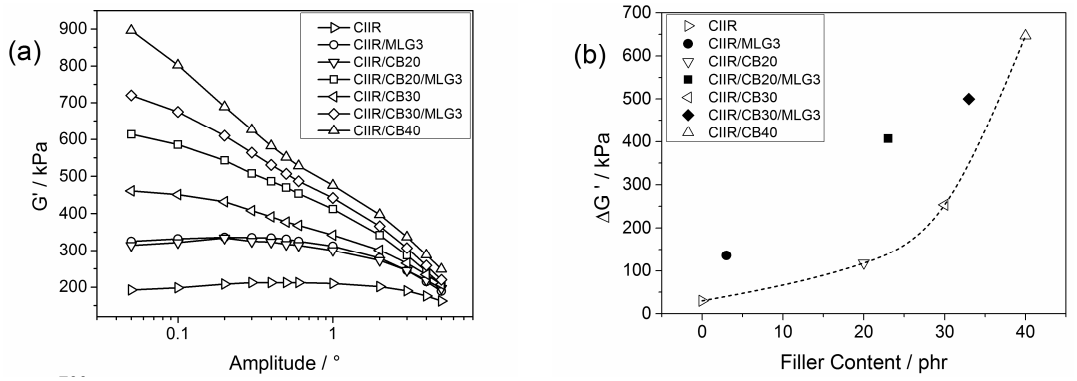

Figure 5. (**a**) Storage modulus as a function of the strain amplitude of CIIR and its composites; and (**b**) difference between initial and final storage modulus as a function of the filler content; the line is a visual guide.

Figure 5b reports the difference between the maximum and minimum of G′ as a function of the filler content. ΔG′ of CIIR/MLG3 was 136 kPa, which is in correspondence with 23 phr CB. Adding 3 phr MLG/20 phr CB shows the largest increase in ΔG (around 300 kPa) and thus reinforced ΔG′ as much as adding 32 phr CB; consequently the effect of 3 phr MLG was similar to 12 phr CB. In the presence of 30 phr CB, the effect of 3 phr MLG corresponded to 7 phr CB. Due to the non-linear behaviour of ΔG′ *versus* CB content, the efficiency of adding 3 phr MLG with respect to replacing CB decreased markedly with higher CB content.

3.3. Curing Properties

The curing curves of CIIR and its composites with MLG and CB are reported in Figure 6a. Vulcanization results in an increase of the torque over time. MLG and CB reinforced the torque and thus the curves of the filled compound were higher than CIIR.

Figure 6b reports the maximum of torque (MH) as a function of the filler content. MH is a measure of the stock modulus of the cured compounds [39]. Adding 3 phr MLG increases the MH of the composites by 1 to 2 dNm. Adding 3 phr MLG increased the MH of CIIR as much as 16 phr CB. In the presence of 20 and 30 phr CB, the reinforcing effect of 3 phr MLG was similar to 12 phr CB.

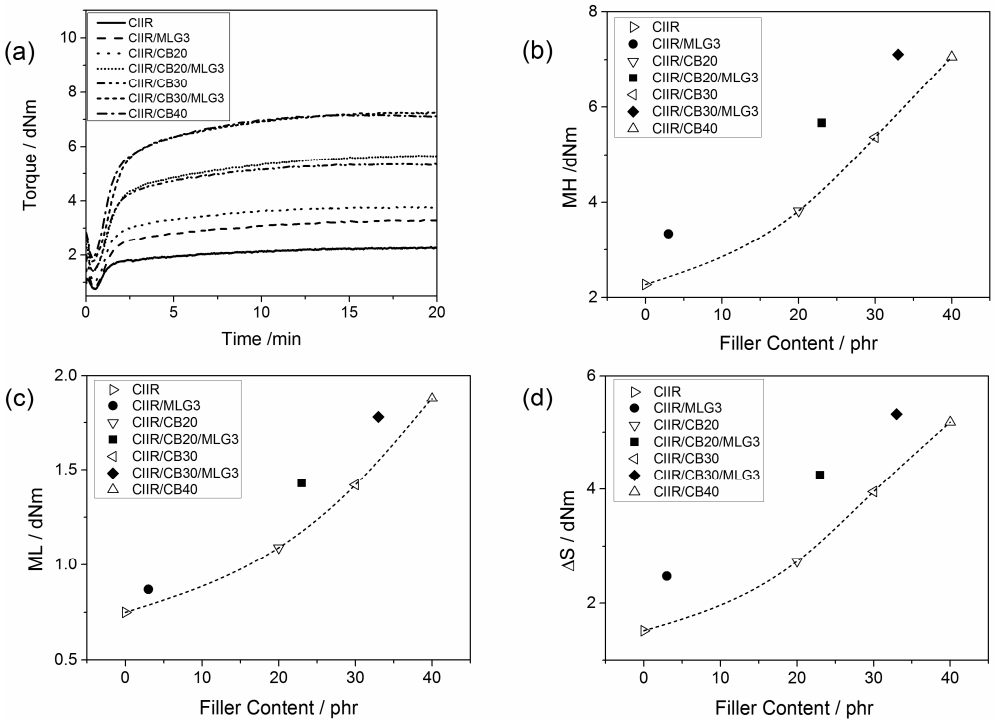

Figure 6. (**a**) Curing curves of CIIR (chlorine isobutyl isoprene rubber) and its composites; (**b**) maximum of the torque; (**c**) minimum of the torque; and (**d**) difference between maximum and minimum of the torque as a function of the filler content; the lines are visual guides.

Figure 6c shows the minimum of the torque (ML) as a function of the filler loading. ML is a measure of the viscosity of the uncured compounds [40]. Adding 3 phr MLG increased the ML of CIIR by 14 %, which matched the effect of 10 phr CB. A similar effect was recorded in the presence of 20 phr CB. In the case of CIIR/CB30/MLG3, the nanofiller reinforced like 8 phr CB.

The difference between MH and ML (ΔS) is usually assumed to be proportional to the cross-link density [41,42]. ΔS is plotted as function of the filler content in Figure 6d. Adding 3 phr MLG increased ΔS by 1 to 1.4 dNm. As for MH, the effect of 3 phr MLG in CIIR/MLG was similar to 16 phr CB. The presence of 20 and 30 phr CB in CIIR/MLG/CB nanocomposite showed the same effect as adding an additional 12 phr CB. The curing properties of CIIR and its composites are summarized in Table 3.

Table 3. Curing properties of CIIR and its composites.

	ML (dNm)	MH (dNm)	ΔS (dNm)
CIIR	0.75 ± 0.01	2.27 ± 0.01	1.52 ± 0.02
CIIR/MLG3	0.87 ± 0.03	3.34 ± 0.02	2.47 ± 0.05
CIIR/CB20	1.09 ± 0.06	3.82 ± 0.06	2.73 ± 0.01
CIIR/CB20/MLG3	1.43 ± 0.01	5.67 ± 0.01	4.25 ± 0.01
CIIR/CB30	1.42 ± 0.01	5.37 ± 0.01	3.95 ± 0.02
CIIR/CB30/MLG3	1.79 ± 0.10	7.11 ± 0.21	5.32 ± 0.11
CIIR/CB40	1.88 ± 0.04	7.06 ± 0.16	5.18 ± 0.20

3.4. Morphology of the CIIR and its Composites

Figure 7 shows the SEM micrographs of the freeze-fractured surface of CIIR and its composites. The surface of CIIR was smooth (Figure 7a). The incorporation of 3 phr MLG resulted in an increase in roughness of the surface of the investigated rubber (Figure 7b). In contrast, the surface of CIIR/CB20 presented few and large protuberances, but was completely smooth at high magnifications (Figure 7c).

CIIR/CB20/MLG3 and CIIR/CB30/MLG/3 had a rough surface (Figure 7f). The small protuberances, visible at higher magnifications, were attributed to the MLG wrapped by a layer of rubber [43,44]. In fact, they are also presented on the surface of CIIR/MLG3. The surfaces of CIIR/CB30 and CIIR/CB40 were also rough (Figure 7e,g). As for CIIR/CB20, they were almost smooth at higher magnifications. Agglomerates were not detected on the fractured surfaces of the CIIR composites because the fillers were well dispersed in the elastomeric matrix.

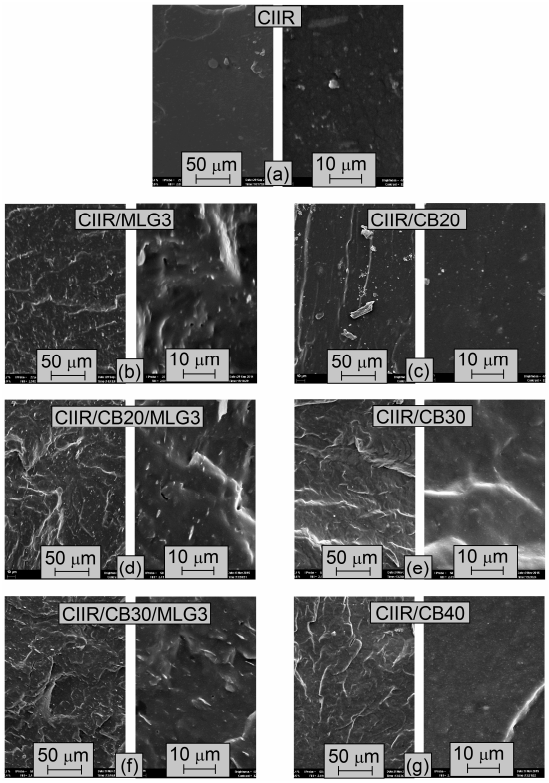

Figure 7. (**a**)–(**g**) SEM micrographs of CIIR and its composites.

During the preparation of the nanocomposites the particles of MLG (Figure 1a–c) were broken apart completely. Then the single MLG stacks were homogenously dispersed in the elastomeric matrix as shows the TEM micrograph of CIIR/MLG3 (Figure 8a), where the black lines were identified as MLG while the black spots were allocated to CB and zinc oxide. Moreover any prevalent orientation was detected.

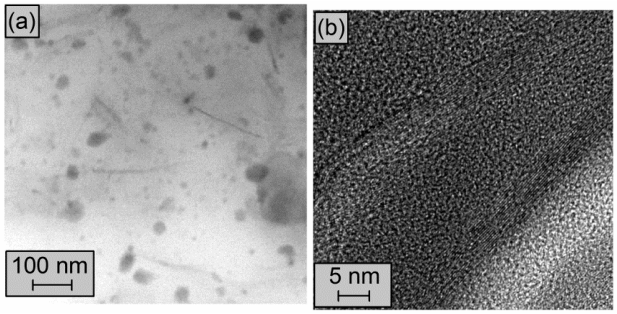

Figure 8. (**a**) and (**b**) TEM micrographs of CIIR/MLG3.

The TEM micrograph in Figure 8b shows two MLG stacks, which consist of 12 graphene sheets. Examining the TEM micrographs the approximate dimensions of the dispersed MLG were determined:

5 ± 2 nm of thickness and 170 ± 60 nm of width. Therefore the average aspect ratio of MLG in CIIR nanocomposite was 34.

3.5. Mechanical Properties

The stress-strain curves of CIIR and its composites are reported in Figure 9a. The mechanical properties of the elastomer were reinforced by CB and MLG; thus the composites were stiffer than CIIR. The shape of the curves for CIIR/CB20, CIIR/CB30 and CIIR/CB40 is almost the same: a gentle increase in the stress at low elongation and a strong one at high elongation. On the other hand, the curves of CIIR/CB20/MLG3 and CIIR/CB30/MLG3 are almost linear. CIIR/CB20/MLG3 and CIIR/CB30/MLG3 were the stiffest composites. Moreover, up to 400% elongation the stresses of CIIR/MLG3 and CIIR/CB20 were very similar and CIIR/CB30/MLG3 presented the highest stress up to 450% elongation.

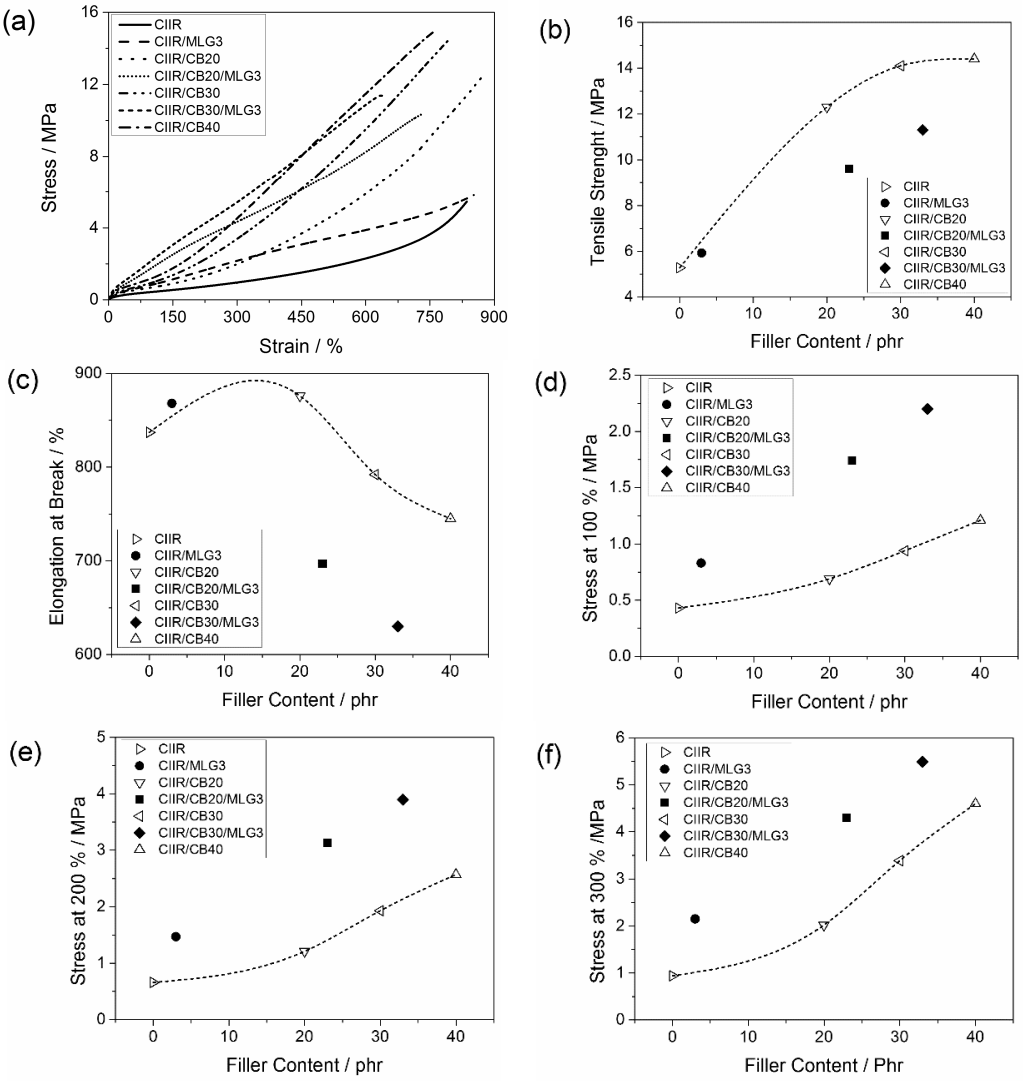

Figure 9. (**a**) Tensile stress *vs.* strain curves and of CIIR and its composites; (**b**) tensile strength; (**c**) elongation at break; (**d**) stress at 100% of elongation; (**e**) stress at 200% of elongation; and (**f**) stress at 300% of elongation as functions of the filler content. The lines are visual guides.

In Figure 9c–f, the mechanical properties were plotted as function of filler loading. The final tensile strength of CIIR was not significantly increased by 3 phr MLG, while it was strongly increased by 20 and 30 phr CB (Figure 9b). The effect of 30 phr CB was very similar to 40 phr CB. The combinations of

CB and MLG also resulted in a higher tensile strength of CIIR, but this increase was lower than the effect of 20 phr CB. CIIR/CB20/MLG3 presented a tensile strength like a compound with 10 phr CB, while the combination of 30 phr CB and 3 phr MLG reinforced the tensile strength as much as about 15 phr CB.

Figure 9c shows the elongation at break as a function of the filler content. Adding 3 phr MLG and 20 phr CB resulted in a small increase in the final elongation, while the compounds with higher filler loading were more brittle. The reduction in elongation at break due to 3 phr MLG plus 20 phr CB was similar to that in composites with more than 50 phr CB. The strongest reduction was obtained with the simultaneous presence of 3 phr MLG and 30 CB. Based on a rough extrapolation, it was similar to more than 65 phr CB.

The effect of the 3 phr on the stress at 100 % was very strong, as shown in Figure 9d. The stress at 100% of CIIR/MLG3 was the same as for a CIIR compound with 25 phr CB. The reinforcement of 3 phr MLG was even stronger in the presence of CB. The stress was increased by up to more than a factor 2 when comparing CIIR/MLG/30 phr CB with CIIR/30 phr CB. Using a rough extrapolation, the combination of 3 phr MLG with 20 phr CB and 30 phr reinforced to the same degree as more than 55 phr CB and more than 65 phr, respectively.

A similarly strong increase in stress by up to more than a factor of 2 was observed for 200% elongation, when CIIR/MLG/ CB was compared with CIIR/ CB for 20 phr CB and 30 phr CB. The stress at 200% of CIIR/MLG3 was similar to a composite with 25 phr CB (Figure 9e). The simultaneous reinforcement of 3 phr MLG and 20 phr was probably similar to more than 45 phr CB. The stress at 200% of CIIR/CB30/MLG3 was roughly the same of a composite with more than 55 phr CB.

Figure 9f shows the stresses at 300% as a function of the filler content. Adding 3 phr MLG increases the stress by a factor of *ca*. 2. The stress at 300% of CIIR/MLG3 was the same as for compounds with 21 phr CB. In combination of 20 and 30 phr CB, 3 phr MLG improved the stress at 300% like 17 phr CB.

Figure 10 shows the stress-strain curves to determine the Young's modulus of CIIR and its composites. The Young's modulus is the slope of the curves and it was increased by adding CB and MLG. In Figure 10b the elastic moduli are plotted as a function of the filler content. Adding 3 phr MLG tripled the Young's modulus of CIIR. Thus 3 phr MLG reinforced CIIR as much as adding 20 phr CB (Figure 9b). An amount of 3 phr MLG in CIIR/CB composites reinforced the Young's modulus by 2.8 MPa and 5.7 MPa for CIIR/20 phr CB and CIIR/30 phr CB, respectively. They match the effect of adding 17 phr CB in addition to the 20 and 30 phr CB.

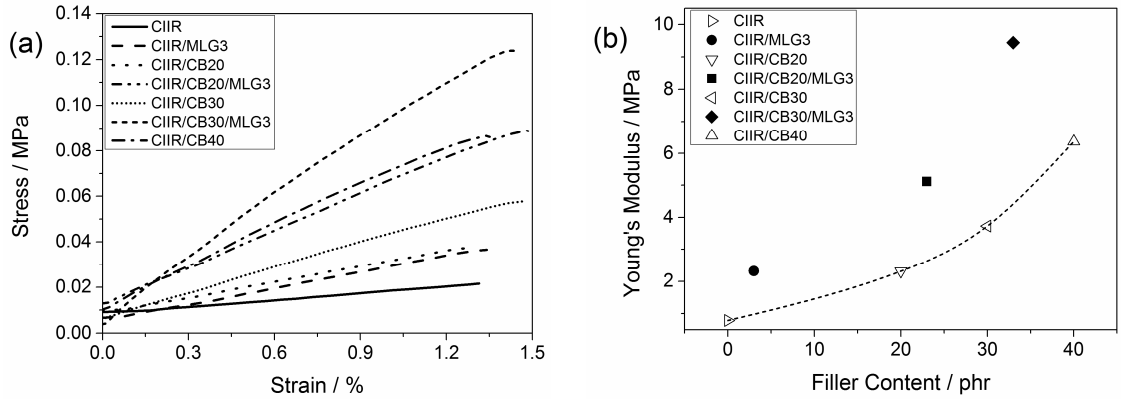

Figure 10. (**a**) Stress *vs.* strain curves to determine Young's modulus of CIIR and its composites; and (**b**) Young's modulus as a function of the filler content. The line is a visual guide.

Figure 11 reports the hardness of CIIR and its composites as a function of filler content. The hardness of CIIR of 12 Shore A was increased by just 3 phr MLG. This effect was similar to that of 17 phr CB. MLG also strongly reinforced the rubber in the presence of CB. In fact, the hardness of CIIR/CB20/MLG3 (53 Shore A) was very similar to the hardness of CIIR/CB40 (54 Shore A).

The increase in Shore A hardness was linear with CB content and quite constant (13.8 ± 1.1) when adding 3 phr MLG. Hence, in the case of hardness, 3 phr MLG replaced about 20 phr CB in all of the nanocomposites. CIIR/CB30/MLG3 was the hardest compound. The mechanical properties of CIIR and its composites are summarized in Table 4.

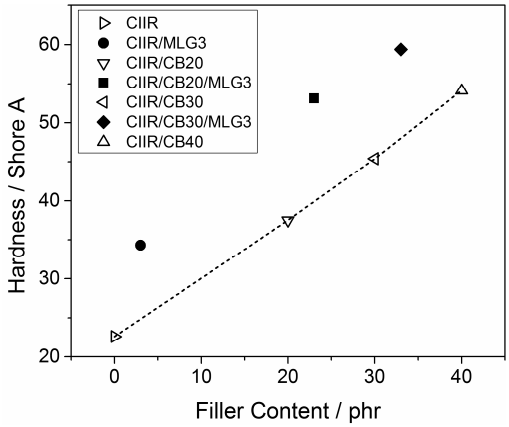

Figure 11. Hardness of CIIR and its composites as a function of the filler content; the line is a visual guide.

Table 4. Mechanical properties of CIIR and its composites.

	Stress 100%/MPa	Stress 200%/MPa	Stress 300%/MPa	Tensile strength/MPa
CIIR	0.43 ± 0.01	0.66 ± 0.03	0.94 ± 0.04	5.28 ± 0.89
CIIR/MLG3	0.83 ± 0.01	1.47 ± 0.02	2.15 ± 0.03	5.93 ± 0.29
CIIR/CB20	0.69 ± 0.01	1.21 ± 0.02	2.02 ± 0.04	12.30 ± 0.51
CIIR/CB20/MLG3	1.74 ± 0.03	3.13 ± 0.05	4.30 ± 0.05	9.62 ± 0.81
CIIR/CB30	0.94 ± 0.02	1.93 ± 0.04	3.39 ± 0.08	14.10 ± 0.68
CIIR/CB30/MLG3	2.20 ± 0.06	3.90 ± 0.08	5.49 ± 0.96	11.30 ± 0.74
CIIR/CB40	1.21 ± 0.01	2.57 ± 0.04	4.60 ± 0.06	14.40 ± 0.28
	Elongation at break/%	**Young's modulus/MPa**	**Hardness/Shore A**	
CIIR	837 ± 29	0.79 ± 0.22	22.6 ± 0.6	
CIIR/MLG3	868 ± 26	2.32 ± 0.08	34.3 ± 0.9	
CIIR/CB20	876 ± 20	2.31 ± 0.11	37.5 ± 0.3	
CIIR/CB20/MLG3	697 ± 46	5.12 ± 0.18	53.1 ± 0.4	
CIIR/CB30	792 ± 25	3.73 ± 0.05	45.4 ± 0.4	
CIIR/CB30/MLG3	630 ± 38	9.44 ± 0.43	59.4 ± 0.5	
CIIR/CB40	745 ± 16	6.37 ± 0.25	54.1 ± 0.6	

3.6. Dynamic Mechanical Properties

The dynamic mechanical properties of CIIR and its compounds are shown in Figure 12. The storage modulus (G′) as a function of the temperature is reported in Figure 12a. The reinforcing effect of the tested fillers resulted in an increase of G′ in the solid state at low temperatures as well as in the rubber state at temperatures above −30 °C. In all temperature ranges, the G′ of CIIR/MLG3 and CIIR/CB20 are almost identical. Higher filler content results in a higher increase in G′. Figure 12b reports G′ at 25 °C as a function of the filler content. At this temperature, the G′ of CIIR/MLG3 was increased by more than a factor of 2 compared to the G′ of CIIR, and thus presented the same G′ as a CIIR compound with 23 phr CB. In combination with 20 and 30 phr CB, 3 phr MLG also increased the G´ by more than a factor of 2, which corresponds to the increase in G′ at 25 °C for adding another *ca*. 13 phr CB.

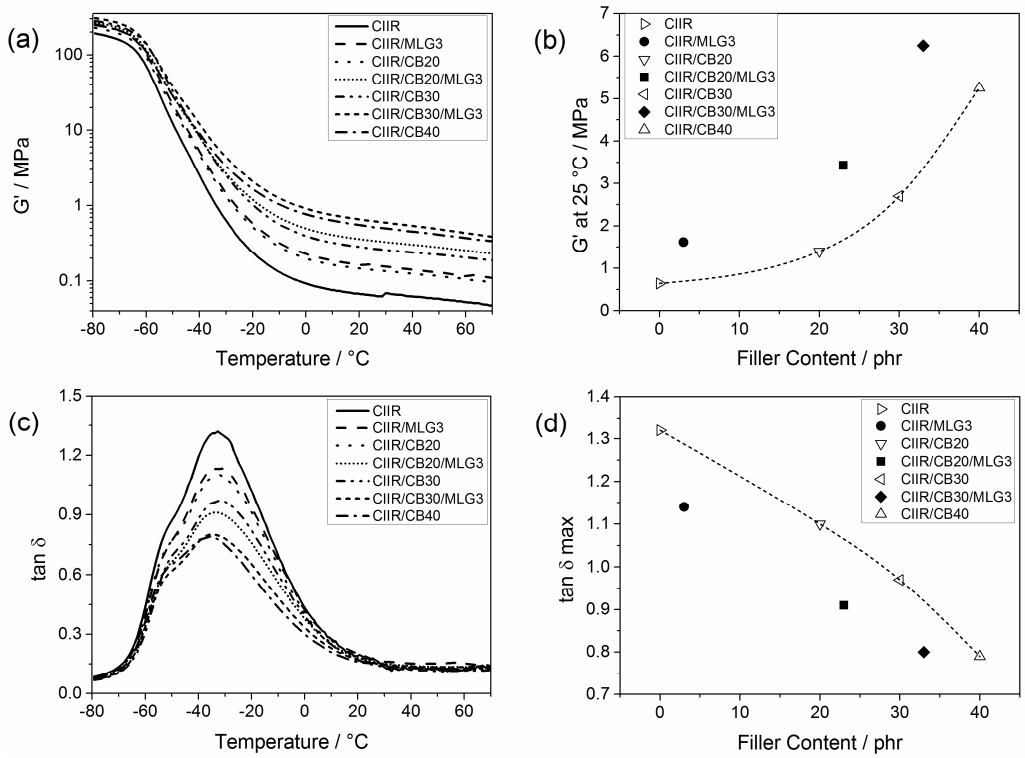

Figure 12. (**a**) Storage modulus of CIIR and its composites as a function of the temperature; (**b**) storage modulus at 25 °C as a function of the filler content—the line is a visual guide; (**c**) tan δ of CIIR and its composites as a function of temperature; and (**d**) maximum of tan η as a function of the filler content—the line is a visual guide.

Figure 12c reports the loss factor peak (tan δ of CIIR and its composites. The presence of fillers resulted in a reduction in the height of the peak because the fillers decreased the elastomeric chain mobility [45]. Strong rubber–filler interactions are the reasons for this behavior [46,47].

The maximum of tan δ as a function of the filler loading is reported in Figure 11d. The effect of 3 phr MLG was the same as of 16 phr CB. Adding 3 phr MLG reduced the maximum of tan δ of CIIR like 13 phr CB in the presence of 20 phr CB, while in the case of CIIR/CB30/MLG3, 3 phr MLG acted like 10 phr MLG.

3.7. Durability of Mechanical Properties Against Weathering Exposure

Figure 13 shows the tensile strength of CIIR and its composites with MLG and CB as a function of the weathering. In the case of unfilled CIIR the tensile strength was reduced by 34% after 1000 h and by 49% after 1500 h. The combination of oxidative gases and UV degrades the CIIR through multi-step photo-oxidation [30]. This degradation is the cause of the loss in tensile strength. The CIIR composites reinforced with MLG and CB conserved their initial tensile strength after the weathering/ageing because the two fillers inhibited the photo-oxidation. As described in Section 3.1, MLG and CB absorb UV and act as radical scavengers. These two mechanisms explain the stabilization effect of the carbon particles studied.

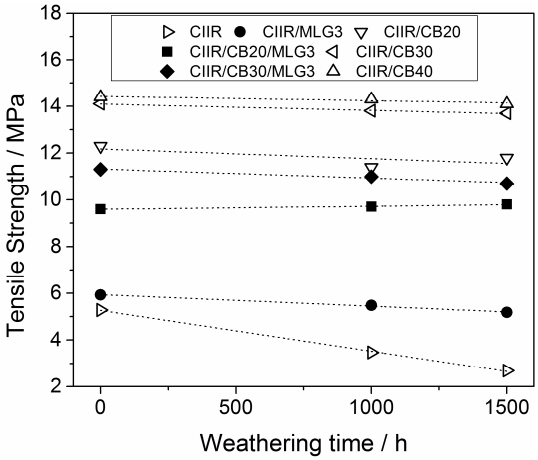

Figure 13. Tensile strength of CIIR and its composites as a function of the weathering/exposure duration time. The lines are visual guides.

4. Conclusions

MLG is a nanoparticle consisting of just approximately 10 graphene sheets and it was proposed as a nanofiller for CIIR in order to partly replace CB. The incorporation of MLG significantly improved the curing, rheological and mechanical properties of CIIR, e.g., just 3 phr CB increased the Young's modulus of CIIR by a factor of 3. Thus, the effect is similar to adding 20 phr CB. The strong reinforcing effect of MLG was also evident in the presence of CB, as shown for a variety of mechanical characteristics in this comprehensive investigation. For instance, the combination of 3 phr MLG and 20 phr CB in CIIR/MLG/20 phr CB increased the Shore A hardness of CIIR by 14 compared to CIIR/20 phr CB, achieving the same hardness as CIIR/40 phr CB. A similarly large impact of adding 3 phr MLG on properties of CIIR/CB composites was observed for all of the properties investigated, which were often improved by a factor of 2 to 3. The influence of 3 phr MLG mostly equals a CB amount of 10–25 phr, sometimes even more. The tested carbon particles absorbed UV, acted as radical scavengers and hence inhibited the weathering degradation of CIIR. Therefore the CIIR composites with MLG and CB conserved their initial mechanical properties after weathering exposure.

This study proposes the combination of CB composites with MLG nanocomposites as promising route to replace some of the CB as a filler. Rubber/CB/MLG compounds harbor the potential for reducing the filler amount and outperform the rubber/CB composites. It should not escape our notice that the investigation of this potential is not only an academic indulgence, but this is also ready for industrial and commercial exploitation.

Acknowledgments: The authors thank Michael Morys for the SEM micrographs, Christian Huth for the dynamic mechanical measurement, Carsten Vogt for support in the tensile tests, Ilona Dörfel for TEM investigations, Martina Bistritz for assistance with cry microtome and Robert Feher from Graphit-Kropfmühl/AMG Mining AG for the MLG.

Author Contributions: Daniele Frasca contributed to the concept and design of the approach of this study and its working packages, prepared master batches, materials and specimens, performed experiments, evaluated the data, did the scientific discussion and conclusions, and wrote the paper; Dietmar Schulze contributed to the design of the working packages, to performing experiments, and to the scientific discussion; Volker Wachtendorf contributed to the weathering and UV absorption part of the study; Bernd Krafft prepared the rubber; Thomas Rybak contributed to the ICOT investigation; and Bernhard Schartel contributed to the concept and design of the approach and the working packages, applied for and procured the project, supervised the study, contributed to the scientific discussion and the writing of the paper.

Conflicts of Interest: The authors declare no conflict of interest.

References

1. Araby, S.; Meng, Q.; Zhang, L.; Zaman, I.; Mejewski, P.; Ma, J. Elastomeric composites based on carbon nanomaterials. *Nanotechnology* **2015**, *26*, 112001. [CrossRef] [PubMed]
2. Wolff, S. Chemical aspects of rubber reinforcement by fillers. *Rubber Chem. Technol.* **1996**, *69*, 325–346. [CrossRef]
3. Dannenberg, E.M. The effects of surface chemical interactions on the properties of filler-reinforced rubbers. *Rubber Chem. Technol.* **1975**, *48*, 410–444. [CrossRef]
4. Usuki, A.; Kojima, Y.; Kawasumi, M.; Okada, A.; Fukushima, Y.; Kurauchi, T.; Kamigaito, O. Synthesis of nylon 6-clay hybrid. *J. Mater. Res.* **1993**, *8*, 1179–1184. [CrossRef]
5. Arroyo, M.; López-Manchado, M.A.; Herrero, B. Organo-montmorillonite as substitute of carbon black in natural rubber compounds. *Polymer* **2003**, *44*, 2447–2453. [CrossRef]
6. Conzatti, L.; Stagnaro, P.; Colucci, G.; Bongiovanni, R.; Priola, A.; Lostritto, A.; Galimberti, M. The clay mineral modifier as the key to steer the properties of rubber nanocomposites. *Appl. Clay Sci.* **2012**, *61*, 14–21. [CrossRef]
7. Peng, C.-C.; Göpfert, A.; Drechsler, M.; Abetz, V. "Smart" silica-rubber nanocomposites in virtue of hydrogen bonding interaction. *Polym. Adv. Technol.* **2005**, *16*, 770–782. [CrossRef]
8. Gallo, E.; Schartel, B.; Schmaucks, G.; Von der Ehe, K.; Böhning, M. Effect of well dispersed amorphous silicon dioxide in flame retarded styrene butadiene rubber. *Plast. Rubber Compos.* **2013**, *42*, 34–42. [CrossRef]
9. Peddini, S.K.; Bosnyak, C.P.; Henderson, N.M.; Ellison, C.J.; Paul, D.R. Nanocomposites from styrene-butadiene rubber (SBR) and multiwall carbon nanotubes (MWCNT) part 1: Morphology and rheology. *Polymer* **2014**, *55*, 258–270. [CrossRef]
10. Das, A.; Stöckelhuber, K.W.; Jurk, R.; Saphiannikova, M.; Fritzsche, J.; Lorenz, H.; Klüppel, M.; Heinrich, G. Modified and unmodified multiwalled carbon nanotubes in high performance solution-styrene-butadiene and butadiene rubber blends. *Polymer* **2008**, *49*, 5276–5283. [CrossRef]
11. Galimberti, M.; Coombs, M.; Cipolletti, V.; Spatola, A.; Guerra, G.; Lostritto, A.; Giannini, L.; Pandini, S.; Riccò, T. Delaminated and intercalated organically modified montmorillonite in poly(1,4-cis-isoprene) matrix. Indications of counterintuitive dynamic-mechanical behavior. *Appl. Clay Sci.* **2014**, *97–98*, 8–16. [CrossRef]
12. Galimberti, M.; Coombs, M.; Cipolletti, V.; Giannini, L.; Conzatti, L. The origin of synergism between an organoclay and carbon black. *Appl. Clay Sci.* **2013**, *83*, 449–456. [CrossRef]
13. Galimberti, M.; Coombs, M.; Cipolletti, V.; Riccio, P.; Riccò, T.; Pandini, S.; Conzatti, L. Enhancement of mechanical reinforcement due to hybrid filler networking promoted by an organoclay in hydrocarbon-based nanocomposites. *Appl. Clay Sci.* **2012**, *65*, 57–66. [CrossRef]
14. Forouharshad, M.; Gardella, L.; Furfaro, D.; Galimberti, M.; Monticelli, O. A low-environmental-impact approach for novel bio-composites based on PLLA/PCL blends and high surface area graphite. *Eur. Polym. J.* **2015**, *70*, 28–36. [CrossRef]
15. Lapa, V.L.D.C.; de Oliveira, P.D.; Visconte, L.L.Y.; Nunes, R.C.R. Investigation of NBR-cellulose ii nanocomposites by rheometric and equilibrium swelling properties. *Polym. Bull.* **2008**, *60*, 281–290. [CrossRef]
16. Novoselov, K.S.; Geim, A.K.; Morozov, S.V.; Jiang, D.; Zhang, Y.; Dubonos, S.V.; Grigorieva, I.V.; Firsov, A.A. Electric field effect in atomically thin carbon films. *Science* **2004**, *306*, 666–669. [CrossRef] [PubMed]
17. Schopp, S.; Thomann, R.; Ratzsch, K.F.; Kerling, S.; Altstädt, V.; Mülhaupt, R. Functionalized graphene and carbon materials as components of styrene-butadiene rubber nanocomposites prepared by aqueous dispersion blending. *Macromol. Mater. Eng.* **2014**, *299*, 319–329. [CrossRef]
18. Sadasivuni, K.K.; Ponnamma, D.; Thomas, S.; Grohens, Y. Evolution from graphite to graphene elastomer caposites. *Prog. Polym. Sci.* **2014**, *39*, 749–780. [CrossRef]
19. Lee, J.H.; Shin, D.W.; Makotchenko, V.G.; Nazarov, A.S.; Fedorov, V.E.; Yoo, J.H.; Yu, S.M.; Choi, J.-Y.; Kim, J.M.; Ji-Beom, Y. The superior dispersion of easily soluble graphite. *Small* **2010**, *6*, 58–62. [CrossRef] [PubMed]
20. Boehm, H.P.; Clauss, A.; Fischer, G.O.; Hofmann, U. Das adsorptionsverhalten sehr dünner kohlenstoff-folien. *Z. Anorg. Allg. Chem.* **1962**, *316*, 119–127. [CrossRef]

21. Steurer, P.; Wissert, R.; Thomann, R.; Mülhaupt, R. Functionalized graphenes and thermoplastic nanocomposites based upon expanded graphite oxide. *Macromol. Rapid Commun.* **2009**, *30*, 316–327. [CrossRef] [PubMed]
22. Dittrich, B.; Wartig, K.A.; Hofmann, D.; Mülhaupt, R.; Schartel, B. The influence of layered, spherical, and tubular carbon nanomaterials' concentration on the flame retardancy of polypropylene. *Polym. Compos.* **2015**, *36*, 1230–1241. [CrossRef]
23. Dittrich, B.; Wartig, K.A.; Mülhaupt, R.; Schartel, B. Flame-retardancy properties of intumescent ammonium poly(phosphate) and mineral filler magnesium hydroxide in combination with graphene. *Polymers* **2014**, *6*, 2875–2895. [CrossRef]
24. Dittrich, B.; Wartig, K.A.; Hofmann, D.; Mülhaupt, R.; Schartel, B. Carbon black, multiwall carbon nanotubes, expanded graphite and functionalized graphene flame retarded polypropylene nanocomposites. *Polym. Adv. Technol.* **2013**, *24*, 916–926. [CrossRef]
25. Dittrich, B.; Wartig, K.-A.; Hofmann, D.; Mülhaupt, R.; Schartel, B. Flame retardancy through carbon nanomaterials: Carbon black, multiwall nanotubes, expanded graphite, multi-layer graphene and graphene in polypropylene. *Polym. Degrad. Stab.* **2013**, *98*, 1495–1505. [CrossRef]
26. Frasca, D.; Schulze, D.; Böhning, M.; Krafft, B.; Schartel, B. Multilayer graphene chlorine isobutyl isoprene rubber nanocomposites: Influence of the multilayer graphene concentration on physical and flame-retardants properties. *Rubber Chem. Technol.* **2016**, in press. [CrossRef]
27. Frasca, D.; Schulze, D.; Wachtendorf, V.; Huth, C.; Schartel, B. Multifunctional multilayer graphene/elastomer nanocomposites. *Eur. Polym. J.* **2015**, *71*, 99–113. [CrossRef]
28. Wu, J.; Huang, G.; Pan, Q.; Zheng, J.; Zhu, Y.; Wang, B. An investigation on the molecular mobility through the glass transition of chlorinated butyl rubber. *Polymer* **2007**, *48*, 7653–7659. [CrossRef]
29. Frasca, D.; Schulze, D.; Wachtendorf, V.; Morys, M.; Schartel, B. Multilayer graphene/chlorune-isobutene -isoprene rubber nanocomposites: Effect of the dispersion. *Polym. Adv. Technol.* **2016**. in press. [CrossRef]
30. Mertz, G.; Hassouna, F.; Leclère, P.; Dahoun, A.; Toniazzo, V.; Ruch, D. Correlation between (nano)-mechanical and chemical changes occurring during photo-oxidation of filled vulcanised styrene butadiene rubber (SBR). *Polym. Degrad. Stab.* **2012**, *97*, 2195–2201. [CrossRef]
31. Schröder, H.; Zeynalov, E.; Bahr, H.; Rybak, T. Analysing the content of antioxidants in pp materials. *Polym. Polym. Compos.* **2002**, *10*, 73–82.
32. Mensah, B.; Kumar, D.; Lim, D.-K.; Kim, S.G.; Jeong, B.-H.; Nah, C. Preparation and properties of acrylonitrile–butadiene rubber–graphene nanocomposites. *J. Appl. Polym. Sci.* **2015**, *132*, 42457. [CrossRef]
33. Lai, Q.; Zhu, S.; Luo, X.; Zou, M.; Huang, S. Ultraviolet-visible spectroscopy of graphene oxides. *Advances* **2012**, *2*, 032146. [CrossRef]
34. Jäger, C.; Henning, T.; Schlögl, R.; Spillecke, O. Spectral properties of carbon black. *J. Non-Cryst. Solids* **1999**, *258*, 161–179. [CrossRef]
35. Zeynalov, E.B.; Allen, N.S.; Salmanova, N.I. Radical scavengering efficiency of different fullerenes c60–c70 and fullerene soot. *Polym. Degrad. Stab.* **2009**, *94*, 1183–1189. [CrossRef]
36. Kumar, V.; Hanel, T.; Giannini, L.; Galimberti, M.; Giese, U. Graphene reinforced synthetic isoprene rubber nanocomposites. *KGK* **2014**, *10*.
37. Payne, A.R. The dynamic properties of carbon black-loaded natural rubber vulcanizates. *J. Appl. Polym. Sci.* **1962**, *6*, 57–63. [CrossRef]
38. Fritzsche, J.; Lorenz, H.; Klüppel, M. CNT based elastomer-hybrid-nanocomposites with promising mechanical and electrical properties. *Macromol. Mater. Eng.* **2009**, *294*, 551–560. [CrossRef]
39. Teh, P.L.; Mohd Ishak, Z.A.; Hashim, A.S.; Karger-Kocsis, J.; Ishiaku, U.S. Effects of epoxidized natural rubber as a compatibilizer in melt compounded natural rubber–organoclay nanocomposites. *Eur. Polym. J.* **2004**, *40*, 2513–2521. [CrossRef]
40. Malas, A.; Pal, P.; Das, C.K. Effect of expanded graphite and modified graphite flakes on the physical and thermo-mechanical properties of styrene butadiene rubber/polybutadiene rubber (SBR/BR) blends. *Mater. Des.* **2014**, *55*, 664–673. [CrossRef]
41. Ismail, H.; Chia, H.H. The effects of multifunctional additive and epoxidation in silica filled natural rubber compounds. *Polym. Test.* **1998**, *17*, 199–210. [CrossRef]
42. Ismail, H.; Chia, H.H. The effects of multifunctional additive and vulcanization systems on silica filled epoxidized natural rubber compounds. *Eur. Polym. J.* **1998**, *34*, 1857–1863. [CrossRef]

43. Xing, W.; Wu, J.; Huang, G.; Li, H.; Tang, M.; Fu, X. Enhanced mechanical properties of graphene/natural rubber nanocomposites at low content. *Polym. Int.* **2014**, *63*, 1674–1681. [CrossRef]
44. Kang, H.; Zuo, K.; Wang, Z.; Zhang, L.; Liu, L.; Guo, B. Using a green method to develop graphene oxide/elastomers nanocomposites with combination of high barrier and mechanical performance. *Compos. Sci. Technol.* **2014**, *92*, 1–8. [CrossRef]
45. Menes, O.; Cano, M.; Benedito, A.; Giménez, E.; Castell, P.; Maser, W.K.; Benito, A.M. The effect of ultra-thin graphite on the morphology and physical properties of thermoplastic polyurethane elastomer composites. *Compos. Sci. Technol.* **2012**, *72*, 1595–1601. [CrossRef]
46. Das, A.; Kasaliwal, G.R.; Jurk, R.; Boldt, R.; Fischer, D.; Stöckelhuber, K.W.; Heinrich, G. Rubber composites based on graphene nanoplatelets, expanded graphite, carbon nanotubes and their combination: A comparative study. *Compos. Sci. Technol.* **2012**, *72*, 1961–1967. [CrossRef]
47. Poikelispää, M.; Das, A.; Dierkes, W.; Vuorinen, J. The effect of partial replacement of carbon black by carbon nanotubes on the properties of natural rubber/butadiene rubber compound. *J. Appl. Polym. Sci.* **2013**, *130*, 3153–3160. [CrossRef]

4. Summary and Outlook

MLG is a commercially available nanoparticle and it is made of just approximately 10 graphene sheets. In this study it was successfully proposed as nanofiller for rubber nanocomposites and it is ready for a large scale investigation. Only 3 phr of well dispersed MLG improved clearly the performances of the tested elastomers in presence and absence of CB.

Initially CIIR/MLG nanocomposites with the same MLG loading (3 phr) were prepared by means of melt compounding in a two-roll mill, and by an ultrasonically-assisted solution mixing procedure followed by two-roll milling. Rheological measurements, TEM and SEM micrographs showed that the dispersion of MLG was better in the nanocomposites produced via solution. The well dispersed MLG resulted in a high reinforcement in mechanical and curing properties. Beyond the reinforcing effect, the well dispersed MLG showed a protective effect against weathering exposure. In fact the nanocomposites prepared via solution conserved their mechanical properties after weathering exposure. Moreover, ΔS, determined by the curing curves, was proposed as a measure of the dispersion of nanofiller in rubber compounds.

The solution mixing was used to prepare CIIR/MLG nanocomposites with different MLG contents. The high reinforcing effect of the tested nanofiller was evident already at the lowest loading. Just 3 phr of MLG increased clearly the rheological, mechanical, and curing properties compared to the unfilled rubber. Moreover, MLG strongly improved the functional properties of the CIIR: gas impermeability, electrical and thermal conductivities. The increase in thermal conductivity resulted in an increase in the time of ignition. During combustion, MLG formed a protective layer which resulted in improvement to the burning properties. Higher MLG loadings yielded a further improvement in the final properties of the nanocomposites. The comparison between experimental data (Young's modulus and gas

permeability) and theoretical models provided the estimated values of aspect ratio of MLG which were absolutely concordant with the TEM analysis.

The high reinforcing effect was also investigated in others popular rubbers: NR, NBR and SBR. Thus nanocomposites with 3 phr MLG were prepared through the solution mixing procedure followed by two-roll milling. In any rubber, MLG was well dispersed and improved rheological, curing and mechanical properties. Moreover because of its chemical structure, MLG absorbed UV and acted as radical scavenger, inhibiting the photo degradation of the elastomeric matrix. Consequently, the nanocomposites conserved their mechanical properties after weathering exposure.

In the case of CIIR, 3 phr MLG tripled the Young's modulus as 20 phr of CB. The strong reinforcing effect of MLG was also evident in the presence of CB. For instance, the combination of 3 phr MLG and 20 phr CB achieved the same Shore A hardness of 40 phr CB. In all the investigated properties, the influence of 3 phr MLG was mostly equivalent to a CB content of 10 – 25 phr, sometimes even more. The studied carbon particles absorbed UV, acted as radical scavengers and consequently inhibited the photo degradation of CIIR. Thus the CIIR composites with MLG and CB conserved their initial mechanical properties after weathering exposure.

In the end, MLG is an efficient nanofiller for rubbers nanocomposites working already at low content. 3 phr of well dispersed MLG improved clearly the curing, rheological, mechanical and functional properties of the investigated rubber. Moreover the reinforcing effect of 3 phr MLG was similar of 10 – 25 phr of CB. Moreover MLG protected the elastomeric matrices against the weathering exposure.

5. Zusammenfassung

Mehrschichtiges Graphen (MLG) ist ein kommerziell verfügbarer Nanofuellstoff und besteht aus nur ca. 10 Blättern Graphen. In dieser Arbeit wurde MLG erfolgreich als Nanofüllmaterial für Elastomere eingefuehrt und weitreichende Untersuchung vorgenommen. Bereits 3 phr gut verteiltes MLG verbesserte die Leistung der geprüften Elastomere, mit und ohne Carbon Black (CB), deutlich.

Zuerst wurden Chlorbutyl Kautschuk (eng. Chlorine Isobutyl Isoprene Rubber (CIIR)) /MLG-Nanoverbundwerkstoffe mit 3 phr MLG auf zwei unterschiedlicher Arten hergestellt: (i) nur mit einem Duo-Walzwerk, mit zwei parallelen Walzen (ii) mit Ultraschall-gestützten Lösungsmischen gefolgt von dem Duo-Walzwerk. Rheologische Messungen, SEM und TEM Aufnahmen zeigten eine bessere MLG-Dispersion in dem lösungsgemischten Nanoverbundwerkstoff. Gut verteiltes MLG fuehrte zu einer deutlichen Verbesserung der Vulkanisations- und mechanischen Eigenschaften. Zusaetzlich zum Verstärkungseffekt wies gut verteiltes MLG einen Schutzeffekt gegen Bewitterung auf. Tatsaechlich behielten die lösungsgemischten Nanoverbundwerkstoffe ihre mechanischen Eigenschaften nach der Bewitterung bei. Außerdem wurde ΔS (bestimmet durch die Vulkanisationskurven) als Maßeinheit fuer die Dispersion des Nanofüllstoffes in der Gummimischung eingefuehrt.

Anschliessend wurde die erprobte Vorgehensweise mittels Lösungsmischens auch für die Herstellung einer Konzentrationsreihe von CIIR/MLG-Nanoverbundwerkstoffe mit unterschiedlicher MLG-Konzentration verwendet. Bereits bei geringer Füllstoffkonzentration war MLG ein hocheffizientes Nanofüllmaterial für CIIR. Bereits die niedrigste MLG-Konzentration von 3 phr hat zu einer deutlichen Verbesserung der rheologisch, Vulkanisations- und mechanisch Eigenschaften gefuegrt. Zudem verstaertkte MLG nachhaltig die funktionellen Eigenschaften (Gaspermeation, elektrische Leitfähigkeit und Wärmeleitfähigkeit) von CIIR. Die Erhöhung der Wärmeleitfähigkeit fuehrte zu einer

Verzoegerung der Zündzeit. Waehrend eines Brandes bildete MLG eine Schutzschicht aus und verbesserte dadurch das Abbrandverhalten. Der Vergleich von experimentellen Daten (Elastizitätsmodul und Gaspermeation) mit den theoretischen Modellen lieferte geschätzten Werte des Seitenverhältnisses von MLG, die mit der TEM-Analyse uebereinstimmten.

Der festgestellte Verstärkungseffekt wurde auch in anderen weitverwendeten Gummisorten untersucht: Naturkautschuk (eng. Natural Rubber (NR)), Nitril-Butadienkautschuk (eng. Nitrile Butadiene Rubber (NBR)) und Styrol-Butadienkautschuk (eng. Styrene Butadiene Rubber (SBR). Auch diese Nanoverbundwerkstoffe wurden aufgrund der besseren MLG-Dispersion mittels Lösungsmischen mit anschließender Bearbeitung im Duo-Walzwerk mit einer Konzentration von 3 phr MLG herstellet. Bei allen Mischungen war MLG gut verteilt und verbesserte die Vulkanisations-, rheologischen und mechanischen Eigenschaften. Aufgrund seiner chemischen Struktur absorbierte MLG die UV-Strahlung, wirkte gleichzeitig als Radikalfänger und schränkte den photochemischen Abbau der Elastomermatrix ein. Folglich behielten die Nanoverbundwerkstoffe ihre mechanischen Eigenschaften nach der Bewitterung bei.

3 phr MLG hat wie auch 20 phr CB den Elastizitätsmodul von CIIR verdreifacht. Der Verstärkungseffekt des MLG war auch in Gegenwart von CB ersichtlich: Zum Beispiel zeigte die Kombination von 3 phr MLG und 20 phr CB die gleiche Härte wie die Mischung mit 40 phr CB. In allen untersuchten Eigenschaften war der Effekt von 3 phr MLG äquivalent zu 10 – 25 phr CB, manchmal sogar noch mehr. Wie auch MLG adsorbierte CB die UV Strahlung, wirkten als Radikalfänger und schränkten folglich den photochemischer Abbau von CIIR ein. Somit konnte nach der Bewitterung der CIIR/CB/MLG-Verbundwerkstoffe kein Verlust ihrer mechanischen Eigenschaften festgestellt werden.

Letztlich ist MLG ein hocheffizientes Nanofüllmaterial für Gummis schon bei geringer Füllstoffkonzentration. 3 phr an gut verteiltem MLG verbesserte die rheologischen,

Vulkanisations-, mechanischen und funktionellen Eigenschaften der untersuchten Gummis deutlich.

6. References

1. Ciullo, P.A.; Hewitt, N. *The rubber formulary*. Noyes Publications/William Andrew Publishing, LLC: Norwich, New York, USA, 1999.
2. Cataldo, F. *Introduzione alla chimica macromolecolare: Chimica della gomma e delle materie plastiche*. Lupi: Roma, IT, 1994.
3. Ciesielski, A. *An introduction to rubber technoloy*. Rapra Technology Limited: Shawbury, Shrewsbury, Shropshire, SY4 4NR, UK, 1999.
4. Sperling, L.H. Cross-linked polymers and rubber elasticity. In *Introduction to physical polymer science, 4th edition*, John Wiley & Sons Ltd: Hoboken, New Jersey, 2006.
5. Ghosh, P.; Katare, S.; Patkar, P.; Caruthers, J.M.; Venkatasubramanian, V.; Walker, K.A. Sulfur vulcanization of natural rubber for benzothiazole accelerated formulations: From reaction mechanisms to a rational kinetic model. *Rubber Chem. Technol.* **2003**, *76*, 592-693.
6. Wu, J.; Xing, W.; Huang, G.; Li, H.; Tang, M.; Wu, S.; Liu, Y. Vulcanization kinetics of graphene/natural rubber nanocomposites. *Polymer* **2013**, *54*, 3314-3323.
7. Wolff, S. Chemical aspects of rubber reinforcement by fillers. *Rubber Chem. Technol.* **1996**, *69*, 325-346.
8. Dannenberg, E.M. The effects of surface chemical interactions on the properties of filler-reinforced rubbers. *Rubber Chem. Technol.* **1975**, *48*, 410-444.
9. Schartel, B.; Wendorff, J.H. Molecular composites for molecular reinforcement: A promising concept between success and failure. *Polym. Eng. Sci.* **1999**, *39*, 128-151.
10. Araby, S.; Meng, Q.; Zhang, L.; Zaman, I.; Mejewski, P.; Ma, J. Elastomeric composites based on carbon nanomaterials. *Nanotechnology* **2015**, *26*, 112001.
11. Rosamma, A. Nanofillers in rubber-rubber blends. In *Rubber nanocomposites: Preparation, properties and applications*, Sabu, T.; Ranimol, S., Eds. John Wiley & Sons Ltd: Chichester, U.K., 2010.
12. Jun, M.; Li Qun, Z.; Li, G. Manufacturing techniques of rubber nanocomposites. In *Rubber nanocomposites: Preparation, properties and applications*, Sabu, T.; Ranimol, S., Eds. John Wiley & Sons Ltd: Chichester, U.K., 2010.
13. Kuilla, T.; Bhadra, S.; Yao, D.; Kim, N.H.; Bose, S.; Lee, J.H. Recent advances in graphene based polymer composites. *Prog. Polym. Sci.* **2010**, *35*, 1350-1375.

14. Ward, I.M.; Hadley, D.W. Polymer composites: Macroscale and microscale. In *An introduction to the mechanical properties of solid polymers*, John Wiley & Sons Ltd: Chichester, U.K., 1993.
15. Usuki, A.; Kojima, Y.; Kawasumi, M.; Okada, A.; Fukushima, Y.; Kurauchi, T.; Kamigaito, O. Synthesis of nylon 6-clay hybrid. *J. Mater. Res.* **1993**, *8*, 1179-1184.
16. Gatos, K.G.; Karger-Kocsis, J. Rubber/clay nanocomposites: Preparation, properties and applications. In *Rubber nanocomposites: Preparation, properties and applications,*, Sabu, T.; Ranimol, S., Eds. John Wiley & Sons Ltd: Chichester, U.K., 2010.
17. Manias, E.; Touny, A.; Wu, L.; Strawhecker, K.; Lu, B.; Chung, T.C. Polypropylene/montmorillonite nanocomposites. Review of the synthetic routes and materials properties. *Chem. Mater.* **2001**, *13*, 3516-3523.
18. Okamoto, M. Polymer/layered filler nanocompositees: An overview from science and technology. In *Macromolecular engineering: Precise synthesis, materials properties, applications, 4 volume*, Matyjaszewski, K.; Gnanou, Y.; Leibler, L., Eds. Wiley-VCH Verlag GmbH & Co. KGaA: Weinheim, Germany, 2007.
19. Galimberti, M.; Coombs, M.; Cipolletti, V.; Riccio, P.; Riccò, T.; Pandini, S.; Conzatti, L. Enhancement of mechanical reinforcement due to hybrid filler networking promoted by an organoclay in hydrocarbon-based nanocomposites. *Appl. Clay Sci.* **2012**, *65-66*, 57-66.
20. Galimberti, M.; Coombs, M.; Cipolletti, V.; Giannini, L.; Conzatti, L. The origin of synergism between an organoclay and carbon black. *Appl. Clay Sci.* **2013**, *83-84*, 449-456.
21. Galimberti, M.; Coombs, M.; Cipolletti, V.; Spatola, A.; Guerra, G.; Lostritto, A.; Giannini, L.; Pandini, S.; Riccò, T. Delaminated and intercalated organically modified montmorillonite in poly(1,4-cis-isoprene) matrix. Indications of counterintuitive dynamic-mechanical behavior. *Appl. Clay Sci.* **2014**, *97-98*, 8-16.
22. Komori, Y.; Kuroda, K. Layered silicate-polymer intercalation compounds. In *Polymer-clay nanocomposites*, Pinnavia, T.J.; Beall, G.W., Eds. John Wiley & Sons Ltd.: Chichester, U.K., 2000.
23. Das, A.; Stöckelhuber, K.W.; Jurk, R.; Saphiannikova, M.; Fritzsche, J.; Lorenz, H.; Klüppel, M.; Heinrich, G. Modified and unmodified multiwalled carbon nanotubes in

high performance solution-styrene–butadiene and butadiene rubber blends. *Polymer* **2008**, *49*, 5276-5283.

24. Dittrich, B.; Wartig, K.A.; Hofmann, D.; Mülhaupt, R.; Schartel, B. Carbon black, multiwall carbon nanotubes, expanded graphite and functionalized graphene flame retarded polypropylene nanocomposites. *Polym. Adv. Technol.* **2013**, *24*, 916-926.
25. Kashiwagi, T.; Grulke, E.; Hilding, J.; Groth, K.; Harris, R.; Butler, K.; Shields, J.; Kharchenko, S.; Douglas, J. Thermal and flammability properties of polypropylene/carbon nanotube nanocomposites. *Polymer* **2004**, *45*, 4227-4239.
26. Iijima, S. Helical microtubes of graphitic carbon. *Nature* **1991**, *357*, 56-58.
27. Bokobza, L. Multiwall carbon nanotube elastomer composites: A review. *Polymer* **2007**, *48*, 4907-4920.
28. Thostenson, E.A.; Zhifeng, R.; Tsu-Wie, C. Advances in the science and technology of carbon nanotubes and their composites: A review. *Compos. Sci. Technol.* **2001**, *61*, 1899-1912.
29. Ferri, T.; Frasca, D.; de Fuentas, O.A.; Santucci, R.; Frasconi, M. Spatially oriented and reversible surface assembly of single-walled carbon nanotubes: A strategy based on π-π interactions. *Angew. Chem. Int. Ed.* **2011**, *50*, 7074-7078.
30. Vairavapandian, D.; Vichchulada, P.; Lay, M.D. Preparation and modification of carbon nanotubes: Review of recent advances and applications in catalysis and sensing. *Anal. Chim. Acta* **2008**, *626*, 119-129.
31. Hutchison, J.L.; Kiselev, N.A.; Krinichnaya, E.P.; Krestinin, A.V.; Loufty, R.O.; Morawsky, A.P.; Muradyan, V.E.; Obraztsova, E.D.; Sloan, J.; Terekhov, S.V., *et al.* Double-walled carbon nanotubes fabricated by a hydrogen arc discharge method. *Carbon* **2001**, *39*, 761-770.
32. Dervishi, E.; Li, Z.; Xu, Y.; Saini, V.; Lupu, D.; Biris, A.R. Carbon nanotubes: Synthesis, properties, and applications. *Part. Sci. Technol.* **2009**, *27*, 107-125.
33. Zhang, Y.; Iijima, S. Formation of single-wall carbon nanotubes by laser ablation of fullerenes at low temperature. *Appl. Phys. Lett.* **1999**, *75*, 3087-3089.
34. Endo, M.; Hayashi, T.; Kim, Y.A.; Muramatsu, H. Development and application of carbon nanotubes. *Jpn. J. Appl. Phys., Part 1* **2006**, *45*, 4883-4892.
35. Sadasivuni, K.K.; Ponnamma, D.; Thomas, S.; Grohens, Y. Evolution from graphite to graphene elastomer caposites. *Prog. Polym. Sci.* **2014**, *39*, 749-780.

36. Lee, J.H.; Shin, D.W.; Makotchenko, V.G.; Nazarov, A.S.; Fedorov, V.E.; Yoo, J.H.; Yu, S.M.; Choi, J.-Y.; Kim, J.M.; Ji-Beom, Y. The superior dispersion of easily soluble graphite. *Small* **2010**, *6*, 58-62.
37. Kim, H.; Abdala, A.A.; Macosko, C.W. Graphene/polymer nanocomposites. *Macromolecules* **2010**, *43*, 6615-6530.
38. Novoselov, K.S.; Geim, A.K.; Morozov, S.V.; Jiang, D.; Zhang, Y.; Dubonos, S.V.; Grigorieva, I.V.; Firsov, A.A. Electric field effect in atomically thin carbon films. *Science* **2004**, *306*, 666-669.
39. Lee, C.; Wei, K.; Kysar, J.W.; Hone, J. Measurement of the elastic properties and intrinsic strength of monolayer graphene. *Science* **2008**, *321*, 385-388.
40. Balandin, A.A.; Ghosh, S.; Bao, W.; Calizo, I.; Teweldebrhan, D.; Miao, F.; Lau, C.N. Superior thermal conductivity of single-layer graphene. *Nano Lett.* **2008**, *8*, 902-907.
41. Du, X.; Skachko, I.; Barker, A.; Andrea, E.Y. Approaching ballistic transport in suspended graphene. *Nat. Nanotechnol.* **2008**, *3*, 491-495.
42. Bunch, J.S.; Verbridge, S.S.; Alden, J.S.; van der Zande, A.M.; Parpia, J.M.; Craighead, H.G.; McEuen, P.L. Impermeable atomic membranes from graphene sheets. *Nano Lett.* **2008**, *8*, 2458-2462.
43. Geim, A.K.; Novoselov, K.S. The rise of graphene. *Nat. Mat.* **2007**, *6*, 183-191.
44. Potts, J.R.; Dreyer, D.R.; Bielawski, C.W.; Ruoff, R.S. Graphene-based polymer nanocomposites. *Polymer* **2011**, *52*, 5-25.
45. Li, X.; Cai, W.; An, J.; Kim, S.; Nah, J.; Yang, D.; Piner, R.; Velamakanni, A.; Jung, I.; Tutuc, E., *et al.* Large-area synthesis of high-quality and uniform graphene films on copper foils. *Science* **2009**, *324*, 1312-1314.
46. Papageorgiou, D.G.; Kinloch, I.A.; Young, R.J. Graphene/elastomer nanocomposites. *Carbon* **2015**, *95*, 460-484.
47. Bourlinos, T.; Georgakilas, V.; Zboril, R.; Steriotis, T.A.; Stubos, A.K. Liquid-phase exfoliation of graphite towards solubilized graphenes. *Small* **2009**, *5*, 1841-1845.
48. Hernandez, Y.; Nicolosi, V.; Lotya, M.; Blighe, F.M.; Sun, Z.; De, S.; McGovern, I.T.; Holland, B.; Byrne, M.; Gun'Ko, Y.K., *et al.* High-yield production of graphene by liquid-phase exfoliation of graphite. *Nat. Nanotechnol.* **2008**, *9*, 563-568.
49. Gong, L.; Young, R.J.; Kinloch, I.A.; Riaz, I.; Jalil, R.; Novoselov, K.S. Optimizing the reinforcement of polymer-based nanocomposites by graphene. *ACS Nano* **2012**, *6*, 2086-2095.

50. Young, R.J.; Kinloch, I.A.; Gong, L.; Novoselov, K.S. The mechanics of graphene nanocomposites: A review. *Compos. Sci. Technol.* **2012**, *72*, 1459-1476.
51. Chen, G.; Zhao, W. Rubber/graphite nanocomposites. In *Rubber nanocomposites: Preparation, properties and applications*, Sabu, T.; Ranimol, S., Eds. John Wiley & Sons Ltd: Chichester, U.K., 2010.
52. Lapa, V.L.d.C.; de Oliveira, P.D.; Visconte, L.L.Y.; Nunes, R.C.R. Investigation of nbr-cellulose ii nanocomposites by rheometric and equilibrium swelling properties. *Polym. Bull.* **2008**, *60*, 281-290.
53. Forouharshad, M.; Gardella, L.; Furfaro, D.; Galimberti, M.; Monticelli, O. A low-environmental-impact approach for novel bio-composites based on plla/pcl blends and high surface area graphite. *Eur. Polym. J.* **2015**, *70*, 28-36.
54. Das, A.; Kasaliwal, G.R.; Jurk, R.; Boldt, R.; Fischer, D.; Stöckelhuber, K.W.; Heinrich, G. Rubber composites based on graphene nanoplatelets, expanded graphite, carbon nanotubes and their combination: A comparative study. *Compos. Sci. Technol.* **2012**, *72*, 1961-1967.
55. Fritzsche, J.; Lorenz, H.; Klüppel, M. Cnt based elastomer-hybrid-nanocomposites with promising mechanical and electrical properties. *Macromol. Mater. Eng.* **2009**, *294*.
56. Potts, J.R.; Shankar, O.; Murali, S.; Du, L.; Ruoff, R.S. Latex and two-roll mill processing of thermally-exfoliated graphite oxide/natural rubber nanocomposites. *Compos. Sci. Technol.* **2013**, *74*, 166-172.
57. Yang, J.; Tian, M.; Jia, Q.-X.; Shi, J.-H.; Zhang, L.-Q.; Lim, S.-H.; Yu, Z.-Z.; Mai, Y.-W. Improved mechanical and functional properties of elastomer/graphite nanocomposites prepared by latex compounding. *Acta Mater.* **2007**, *55*.
58. Frasca, D.; Schulze, D.; Wachtendorf, V.; Morys, M.; Schartel, B. Multilayer graphene / chlorune-isobutene-isoprene rubber nanocomposites: Effect of the dispersion. *Polym. Adv. Technol.* **2016**.
59. Malas, A.; Das, C.K.; Das, A.; Heinrich, G. Development of expanded graphite filled natural rubber vulcanizates in presence and absence of carbon black: Mechanical, thermal and morphological properties. *Mater. Des.* **2012**, *39*, 410-417.
60. Ozbas, B.; D. O'Neill, C.; Register, R.A.; Aksay, I.A.; Prud'homme, R.K.; Adamson, D.H. Multifunctional elastomer nanocomposites with functionalized graphene single sheets. *J. Polym. Sci., Part B: Polym. Phys.* **2012**, *50*.

61. Ozbas, B.; Toki, S.; Hsiao, B.S.; Chu, B.; Register, R.A.; Aksay, I.A.; Prud'homme, R.K.; Adamson, D.H. Strain-induced crystallization and mechanical properties of functionalized graphene sheet-filled natural rubber. *J. Polym. Sci., Part B: Polym. Phys.* **2012**, *50*, 718-723.
62. Frasca, D.; Schulze, D.; Wachtendorf, V.; Huth, C.; Schartel, B. Multifunctional multilayer graphene / elastomer nanocomposites *Eur. Polym. J.* **2015**, *71*, 99-113.
63. Frasca, D.; Schulze, D.; Böhning, M.; Krafft, B.; Schartel, B. Multilayer graphene chlorine isobutyl isoprene rubber nanocomposites: Influence of the multilayer graphene concentration on physical and flame-retardants properties. *Rubber Chem. Technol.* **2016**.
64. Zhan, Y.; Wu, J.; Xia, H.; Yan, N.; Fei, G.; Yuan, G. Dispersion and exfoliation of graphene in rubber by an ultrasonically-assisted latex mixing and in situ reduction process. *Macromol. Mater. Eng.* **2011**, *296*, 590-602.
65. Zhan, Y.H.; Lavorgna, M.; Buonocore, G.; Xia, H. Enhancing electrical conductivity of rubber composites by constructing interconnected network of self-assembled graphene with latex mixing. *J. Mater. Chem.* **2012**, *22*, 10464-10468.
66. Kim, H.; Miura, Y.; Macosko, C.W. Graphene/polyurethane nanocomposites for improved gas barrier and electrical conductivity. *Chem. Mater.* **2010**, *22*, 3441-3450.
67. Zaman, I.; Phan, T.T.; Kuan, H.C.; Meng, Q.; La, L.T.B.; Luong, L.; Youssf, O.; Ma, J. Epoxy/graphene platelets nanocomposites with two levels of interface strength. *Polymer* **2011**, *52*, 1603-1611.
68. Zaman, I.; Kuan, H.C.; Meng, Q.; Michelmore, A.; Kawashima, N.; Pitt, T.; Zhang, L.; Gouda, S.; Luong, L.; Ma, J. A facile approach to chemically modified graphene and its polymer nanocomposites. *Adv. Compos. Mater* **2013**, *22*, 2735-2743.